THE HONG KONG
POLYTECHNIC UNIVERSITY
香港理工大學
Pao Yue-kong Library
包玉剛圖書館

## Copyright Undertaking

This thesis is protected by copyright, with all rights reserved.

**By reading and using the thesis, the reader understands and agrees to the following terms:**

1. The reader will abide by the rules and legal ordinances governing copyright regarding the use of the thesis.
2. The reader will use the thesis for the purpose of research or private study only and not for distribution or further reproduction or any other purpose.
3. The reader agrees to indemnify and hold the University harmless from and against any loss, damage, cost, liability or expenses arising from copyright infringement or unauthorized usage.

**IMPORTANT**

If you have reasons to believe that any materials in this thesis are deemed not suitable to be distributed in this form, or a copyright owner having difficulty with the material being included in our database, please contact lbsys@polyu.edu.hk providing details. The Library will look into your claim and consider taking remedial action upon receipt of the written requests.

Pao Yue-kong Library, The Hong Kong Polytechnic University, Hung Hom, Kowloon, Hong Kong

http://www.lib.polyu.edu.hk

# INTERNET OF THINGS DEVICES STABILITY ENHANCEMENT BY NOISE FILTERING AND COLLISION AVOIDANCE

TSOI MAN HO

MPhil

The Hong Kong Polytechnic University

2026

The Hong Kong Polytechnic University

Department of Mechanical Engineering

# Internet of Things Devices Stability Enhancement by Noise Filtering and Collision Avoidance

Tsoi Man Ho

A thesis submitted in partial fulfilment of the requirements for the degree of Master of Philosophy

July 2025

CERTIFICATE OF ORIGINALITY

I hereby declare that this thesis is my own work and that, to the best of my knowledge and belief, it reproduces no material previously published or written, nor material that has been accepted for the award of any other degree or diploma, except where due acknowledgement has been made in the text.

_____

__Tsoi Man Ho_____ (Name of student)

# Abstract

The concept of Internet of Things (IoT) applications has been proposed for decades but has not yet been implemented on a large scale. The reasons may include the high cost of individual wireless devices and the lack of a wireless solution that supports numerous devices with wide coverage while remaining robust against environmental noise. In this thesis, noise-rejection filters and collision-avoidance medium access control (MAC) protocols for IoT applications are investigated, so that the stability of large-scale IoT wireless networks can be improved by applying appropriate filters and MAC schemes.

First, the low-cost wireless component, the surface acoustic wave (SAW) filter, is evaluated. The design and in-house fabrication process of the SAW filter are presented in this report. The detailed effects of interdigital transducer (IDT) variations are investigated by fabricating SAW filters with parametric variations, including the presence of reflectors, IDT length, port separation, and the number of reflectors and IDTs per port. The fabricated SAW filter achieves an insertion loss of less than 3 dB and a return loss of more than 10 dB at 480 MHz without any external lumped elements at the ports for impedance matching.

Second, from a system perspective, among the available low-power wide-area network (LPWAN) IoT solutions, LoRa is one of the most promising options due to its attractive properties of low cost, high energy efficiency, wide coverage, and robustness to interference. However, the existing LoRaWAN MAC only offers a pure ALOHA mechanism designed for low-duty-cycle applications. Severe collisions are therefore expected if a large-scale system is deployed. To address this issue, multiple

MAC schemes incorporating pure ALOHA, slotted ALOHA, and channel activity detection (CAD) are proposed and tested experimentally. The performance of these MAC schemes is evaluated by comparing the packet delivery ratio (PDR). A PDR of almost 100% is achieved by one of the proposed MAC schemes. Finally, the use cases of the tested MAC schemes are discussed.

Third, Chapter 4 synthesizes insights from the previous discussions on filters and MAC protocols to explore their applicability in enhancing the stability of end devices within a commercial context. A long-term deployment project has been initiated in collaboration with a property management company, encompassing 205 end devices and a single gateway across 23 floors of an operational commercial building. The installation of water flood detection sensors aims to provide prompt notifications to the management team, thereby mitigating potential damage to critical infrastructure such as elevators and escalators. This deployment establishes a centralized IoT water flood detection system for commercial use and demonstrates the capability of a stable IoT system employing filters and collision-avoidance MAC schemes.

# Publications arising from the thesis

1. M. H. Tsoi, Y. S. Choy, C.-F. Chow, and S. W. Y. Mung , "Optimization of surface acoustic wave filter performance with 2D FEM simulation and parametric variation" *Microwave Journal*. Dec 2023.
2. M. H. Tsoi, T. H. Ng, D. P. K. Lun, Y. S. Choy and S. W. Y. Mung, "LoRa Data Throughput Enhancement by Slotted Channel Activity Detection," *2020 IEEE Asia-Pacific Microwave Conference (APMC)*, Hong Kong, Hong Kong, 2020, pp. 466-468, doi: 10.1109/APMC47863.2020.9331636.
3. M. Ho Tsoi, Y. Wing Lo, Y. Sze Choy, C. -F. Chow and S. W. Y. Mung, "LoRa Mesh Network With Time-Efficient Medium Utilization for IoT Building Monitoring System," in *IEEE Transactions on Instrumentation and Measurement*, vol. 74, pp. 1-14, 2025, Art no. 9505514, doi: 10.1109/TIM.2025.3545712

# Other Publications

1. M. H. Tsoi, K. M. Wu, J. S. M. Yuen, Y. S. Choy and S. W. Y. Mung, "Compact transmission-line circuit for audio and microwave signals," *2020 IEEE International Conference on Consumer Electronics - Asia (ICCE-Asia)*, Seoul, Korea (South), 2020, pp. 1-3, doi: 10.1109/ICCE-Asia49877.2020.9276949.
2. M. H. Tsoi, T. H. Ng, D. P. K. Lun, Y. S. Choy and S. W. Y. Mung, "Reconfigurable frequency switching and synchronization for noise avoidance in power line communication system," *2020 IEEE International Conference on Consumer Electronics - Asia (ICCE-Asia)*, Seoul, Korea (South), 2020, pp. 1-4, doi: 10.1109/ICCE-Asia49877.2020.9276974.
3. M. H. Tsoi, K. M. Wu, J. S. M. Yuen, Y. S. Choy and S. W. Y. Mung, "Wideband Planar Coupled-Feed Antenna for Internet of Things Applications," *2020 IEEE Asia-Pacific Microwave Conference (APMC)*, Hong Kong, Hong Kong, 2020, pp. 460-462, doi: 10.1109/APMC47863.2020.9331528.
4. T. C. Kwong, S. L. Wong, M. H. Tsoi, C. H. Chetwyn Chan, Y. S. Choy and W. Y. Steve Mung, "An EEG device with synchronization of auditory stimuli," *2020 IEEE International Conference on Consumer Electronics - Asia (ICCE-Asia)*, Seoul, Korea (South), 2020, pp. 1-5, doi: 10.1109/ICCE-Asia49877.2020.9276500.
5. Y. Wing Lo, M. Ho Tsoi, C. -F. Chow and S. W. Y. Mung, "An NB-IoT Monitoring System for Digital Mobile Radio With Industrial IoT Performance and Reliability Evaluation," in *IEEE Sensors Journal*, vol. 25, no. 3, pp. 5337-5348, 1 Feb.1, 2025, doi: 10.1109/JSEN.2024.3512859.

# Acknowledgement

I would like to express my heartfelt gratitude to all those who supported me throughout my research journey.

First and foremost, I would like to thank my chief supervisor, Dr. Choy, for her invaluable guidance, encouragement, and support. I am especially grateful for her role in my admission to the MPhil program as a part-time student, which allowed me to pursue my academic goals alongside my professional commitments.

I would also like to extend my sincere appreciation to Dr. Steve Mung for his mentorship and valuable feedback. His insights have greatly enriched my work, and I am thankful for his support throughout my studies.

I am grateful to my full-time employer, Louis Ng, for his understanding and support during my part-time studies. His encouragement has made it possible for me to balance my professional and academic endeavors.

My thanks also go to my colleagues in the Mechanical Department at The Hong Kong Polytechnic University for their collaborative spirit and support, which have made my time here truly memorable.

I am particularly thankful to the University Research Facility in Materials Characterization and Device Fabrication (UMF) at The Hong Kong Polytechnic University for providing the necessary resources and facilities that were crucial to my research.

Finally, I would like to express my deepest appreciation to my family for their endless love, patience, and belief in my abilities. Their support has been my anchor throughout this journey.

Thank you all for being a part of this important chapter in my life.

# Content Table

# List of figures, tables and abbreviations

List of Figures

List of Tables

# 1. INTRODUCTION

The Internet of Things (IoT) refers to a network formed by physical devices. These devices are connected to the Internet so that data can be exchanged. Typically, IoT devices are connected to the Internet through wireless solutions. Sensor networks and smart homes with automation systems are examples of IoT applications. Nowadays, automation applications are evolving from home- or office-scale deployments to building management systems, and the scale of sensor networks is expanding from campus-level deployments to citywide coverage. Therefore, the application scenarios become more challenging for two main reasons. First, the radio-frequency (RF) noise inside building machine rooms and across cities is much larger in magnitude and more complex than in typical home or office environments. This environmental noise must be filtered so that IoT devices can operate without interference. Second, a larger number of devices leads to heavier traffic, and collisions between valid data frames become more likely. Data collisions between IoT devices should be minimized to achieve reliable data exchange.

The stability of wireless IoT systems is paramount for ensuring reliable communication and efficient operation in various applications. With the increasing deployment of IoT devices in diverse environments, addressing the challenges posed by environmental noise and data collisions becomes critical. One key component in enhancing system stability is the use of RF filters, among which the surface acoustic wave (SAW) filter is a typical example. These filters effectively suppress environmental noise by allowing only the desired frequency components to pass through, thereby minimizing interference from unwanted signals. Their low production cost, compact size, and high quality factor make SAW filters an ideal

choice for IoT applications, ensuring that devices can operate smoothly even in noisy conditions.

Another crucial aspect is the implementation of efficient medium access control (MAC) protocols. These protocols are designed to manage how multiple IoT devices share the same frequency channel, preventing data collisions that can disrupt communication. By strategically coordinating transmissions, MAC protocols enhance the reliability of data exchange, allowing a large number of devices to operate concurrently without significant performance degradation.

Together, RF filters such as SAW devices and robust MAC protocols play essential roles in bolstering the stability of wireless IoT systems, enabling them to function effectively in complex and dynamic environments.

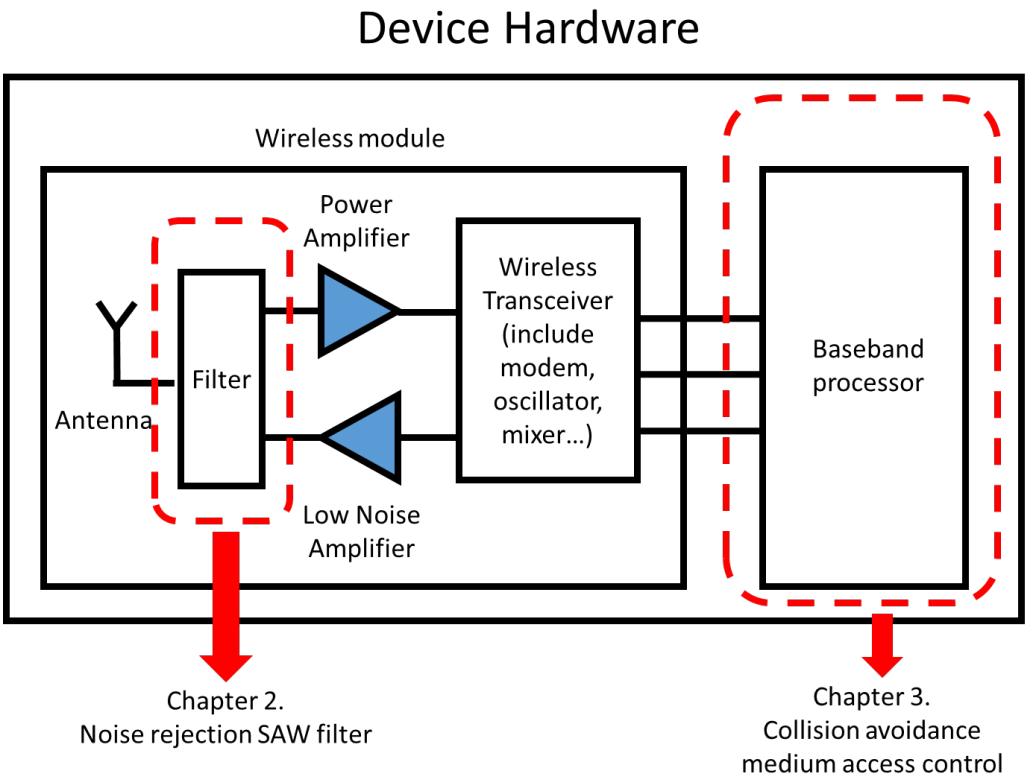


Figure 1.1 Typical hardware block diagram of IoT device.

The hardware block diagram of a wireless device is shown in Figure 1.1. This device comprises an antenna, filters, amplifiers, a transceiver, and a baseband

processor. For clarity, less relevant components have been omitted from the schematic.

## 1.1. RF stability of IoT networks

Surface acoustic wave (SAW) filters are commonly used in existing wireless infrastructure. Their popularity is due to their excellent properties, including a high quality factor, compact size, and low cost. [1]-[2]. As SAW filters can be manufactured using fabrication techniques similar to those used in the semiconductor industry, the cost of mass-producing SAW filters is reduced. [3].

Emerging technologies, such as 5G and the Internet of Things (IoT), further increase the performance demands on filters. Fifth-generation (5G) systems require filters that operate at higher frequency bands, while IoT applications require cheaper and more compact filters [4]-[6]. These requirements may not be fully met by current SAW filter designs; more advanced and refined SAW filters, or even other types of acoustic filters, are needed, such as temperature-compensated SAW devices, bulk acoustic wave (BAW) filters, and XBAR devices. A comprehensive process for future acoustic filter design is therefore of great interest in both research and industry.

Previous advances in physics have already elucidated the working principles of acoustic wave devices, and analytical modeling methods have been established on this basis, such as the coupling-of-modes (COM) model and Green's function methods. [7]-[8]. Such analytical modeling methods are based on assumptions that oversimplify the interdigital transducer (IDT) designs. Therefore, inaccuracies in the modeling, especially in the estimation of the frequency response, are to be expected.

Instead of analytical methods, the finite element method (FEM) is used to capture the detailed design of the IDT. However, 3D FEM modeling is relatively time-consuming, even on computers with high-end hardware. [9].

Moreover, simulation and modeling alone cannot form a complete design cycle. Fabrication and measurement are essential for verifying the accuracy of the simulations. Unfortunately, there is no semiconductor manufacturer in Hong Kong. Sample preparation by overseas third parties increases both development costs and the overall design cycle. The Hong Kong Polytechnic University (PolyU) is one of the few universities in Hong Kong that has the capabilities and facilities to fabricate acoustic devices. As a result, not only design and simulation, but also fabrication and measurement can be carried out within a local university. Fabrication processes that would otherwise take more than a few weeks can be shortened to a few days. Therefore, establishing a standard procedure for designing and fabricating sample acoustic devices represents an attractive direction for university–industry collaboration.

In Chapter 2, the principle of the SAW filter, which is one of the most fundamental acoustic devices, will be reviewed. Then, a complete design cycle consisting of in-house design, simulation, fabrication, and measurement for a bandpass SAW filter with a center frequency of around 480 MHz will be presented. During this design cycle, different parametric variations of the IDT are compared to evaluating their effect on SAW filter performance.

### 1.1.1. Analytical modelling of SAW device performance prediction

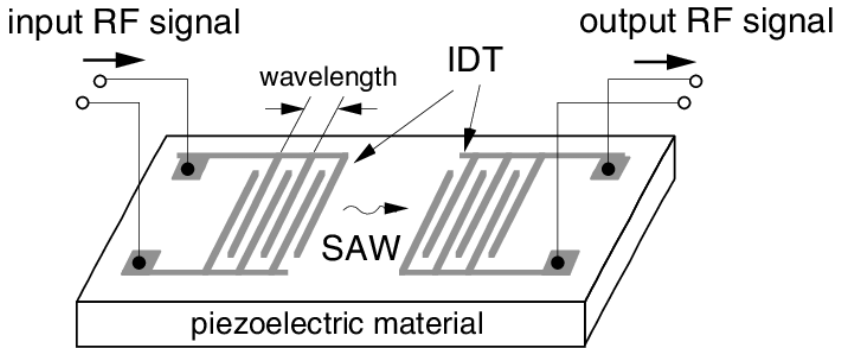


Figure 1.2 Basic configuration of two port SAW filter

The above Figure 1.2 shows the basic elements and working principle of SAW

filter. SAW filter consists of piezoelectric substrate, IDT and reflectors [10].

First, piezoelectric substrates differ from linear elastic materials: when stress is applied to the material, not only is strain induced, but an electric potential is also generated. Conversely, when an electric field is applied, both stress and strain are induced. The piezoelectric properties of the material can be summarized by the following equations. [11]

$$D = [e][S] + [\varepsilon]E \tag{1.1}$$

$$[T] = [c][S] + [e^t]E \tag{1.2}$$

In the above equations, $D$ represents the electric charge density displacement. [$e$] is the piezoelectric coupling coefficient matrix. [$S$] is the strain matrix. [$\varepsilon$] represents dielectric permittivity matrix. $E$ represents the electric field. [$T$] is the stress tensor. [$c$] is the stiffness matrix and [$e^t$] is the transpose of piezoelectric coupling coefficient matrix. The above equation will be same as normal stress strain relation and normal electric displacement electric field if the [$e$] is not present. With the [$e$], the mechanical and electrical property of material are now coupled together.

Second, the interdigital transducer (IDT) is a conductive metallic layer deposited onto the surface of the piezoelectric substrate. The signal and ground pads consist of numerous connected finger-like structures. These pads are placed periodically without crossing each other, and together they form a port. A SAW device may have a single port, functioning as a resonator, or at least two ports, functioning as a filter. For a two-port filter, as depicted in Figure 2.1, when an oscillating electrical signal is applied to Port 1 on the left-hand side, the alternating potential on the pads induces mechanical strain. Because the signal and ground pads are intentionally arranged with a specific periodicity, a mechanical wave, or acoustic wave, with a corresponding frequency is generated on the input port surface. Part of this generated wave propagates along the piezoelectric substrate surface to Port 2 on the right-hand side in Figure 2.1, where the acoustic wave is converted back into an electrical output signal. Since only electrical signals within a specific frequency band can be efficiently converted to acoustic waves at Port 1 and then reconverted to electrical signals at Port 2, this structure functions as

a bandpass filter. The bandpass frequency is governed by the speed of sound of the substrate ($v$) and the pitch of IDTs ($\lambda/2$).

$$v = f\lambda \tag{1.3}$$

The third element is the reflector, which is also a metallic layer but is not connected to the input or output ports. Reflectors are placed to confine Port 1 and Port 2, so that the generated waves are reflected toward Port 2 to reduce losses.

Besides the passband centre frequency, passband insertion loss, passband bandwidth, and stopband rejection are also critical performance indicators of filter performance. However, this information is not clearly revealed in the governing equations. Therefore, the finite element method (FEM) can be applied to equations (1.2) and (1.3) to evaluate the filter performance.

### 1.1.2. Finite Element Method (FEM) of SAW device performance prediction

With the improvement of computing power, FEM simulation has become increasingly feasible. Based on equations (1.1) and (1.2), researchers have investigated the performance of SAW devices [12]-[15]. However, most of these studies have focused on evaluating the accuracy of the mechanical aspects of the simulation, primarily the resonance frequency. This is because their research has mainly targeted SAW resonators and sensors, for which the resonance frequency is the key parameter of interest. Only a few researchers have begun conducting simulations on filters or other two-port SAW devices. [9]. To capture the effects of detailed IDT designs, full 3D simulations with fine mesh are required. However, even with a relatively well-equipped high-end computer, it takes about three days to complete a single frequency sweep for one design. Performing parametric variations of over ten IDT designs, which is still a relatively small number of variations, would therefore require about a month. As a result, relying solely on 3D FEM simulation for SAW filter design may not be the most

effective approach.

3D FEM simulation is the most accurate method for predicting SAW filter performance. However, the time cost makes it impractical for general use. Therefore, 2D FEM simulation is adopted to reduce the computational burden.

In Chapter 2, a hybrid SAW filter design cycle that combines both simulation and fabrication will be presented. First, the IDT design will be discussed. Second, 2D simulations will be performed to quickly estimate the resonance frequency. Because simulation accuracy is partially sacrificed in exchange for reduced computation time, fabrication and measurement are carried out to verify the results.

A key contribution of this chapter is the complete evaluation of the designed SAW filter through simulation, fabrication, and measurement, all performed using in-house equipment. This entire process was conducted on campus exclusively by research students, which significantly reduced the time, cost, and manpower required for the design process, thereby facilitating the advancement of SAW filter design

## 1.2. System stability of IoT networks

The Internet of Things (IoT) enables the remote monitoring, management, and control of devices and environmental conditions in both indoor and outdoor environments through IoT end devices (EDs) [16]. An optimal IoT wireless solution should provide extensive coverage. In addition, the network should be flexible and easily expandable to reach areas that may not be initially accessible.

IoT networks can be established using wired solutions, which generally provide better reliability and coverage than wireless options. Examples include 802.3 Ethernet for surveillance cameras, BACnet for building automation, and DALI for lighting control. These networks can reach any point within a building, provided that data cables are installed. However, wired networks are inflexible and expensive, as data cables

must typically be installed during the design and construction phases. This approach can lead to an excessive number of reserved Ethernet ports for potential future use, many of which may never be needed. Additionally, the locations for installing EDs may not be clearly defined during the initial planning stage.

Once a commercial or residential building is occupied, adding new wiring becomes challenging and often requires closing off certain areas. The cost of data-wiring projects frequently exceeds the cost of the devices themselves. If the wiring must traverse tenant spaces, some tenants may object, causing delays or even halting the project altogether. This inflexibility makes wired solutions less desirable for IoT projects in existing buildings.

In addition to wired options, wireless low-power wide-area network (LPWAN) solutions provide flexibility and cost-effectiveness by eliminating the need for data and power cables for certain battery-operated IoT devices. LPWAN technologies encompass various wireless standards, including Sigfox, Wi-Fi, Long-Term Evolution (LTE) Category M1, Bluetooth Low Energy (BLE), Narrowband IoT (NB-IoT), Zigbee, and Long Range (LoRa). [16]-[17]. Researchers have reviewed and compared current wireless technologies, including LoRa [17] , and have predicted substantial economic impacts as IoT devices shift from short-range to LPWAN solutions. These studies indicate that each technology has unique strengths, suggesting that the choice of technology should depend on the specific application scenario. [18]. Cellular networks like 5G also present a viable alternative to LPWANs, especially where cellular infrastructure is available [19]. While NB-IoT offers enhanced power efficiency compared to traditional cellular networks, it does sacrifice some data speed [20]. LoRa stands out for its long-range capabilities and energy-efficient communication with minimal infrastructure requirements [21].

LPWANs are being explored for various infrastructure monitoring applications,

such as water quality assessment [22], underground infrastructure tracking [23], and campus monitoring [24]. Additionally, LPWANs are being considered for personal health and wellness monitoring, including residential ECG monitoring [25], hospital-level vital sign tracking [26], IoT edge health monitoring with multiple gateways [27], calorie management systems in buffet settings [28], and smart gourmet systems for health monitoring [29].

The advantages of using LPWAN are realized only when the network coverage extends to the locations where new EDs need to be installed. In building monitoring applications, EDs are typically placed in confined areas such as washrooms, staircases, pump rooms, electric meter (EMR) rooms, extra-low-voltage (ELV) rooms, and air-handling unit (AHU) rooms. For personal health and wellness monitoring, EDs may also be deployed in similar locations, including washrooms, staircases, and basements.

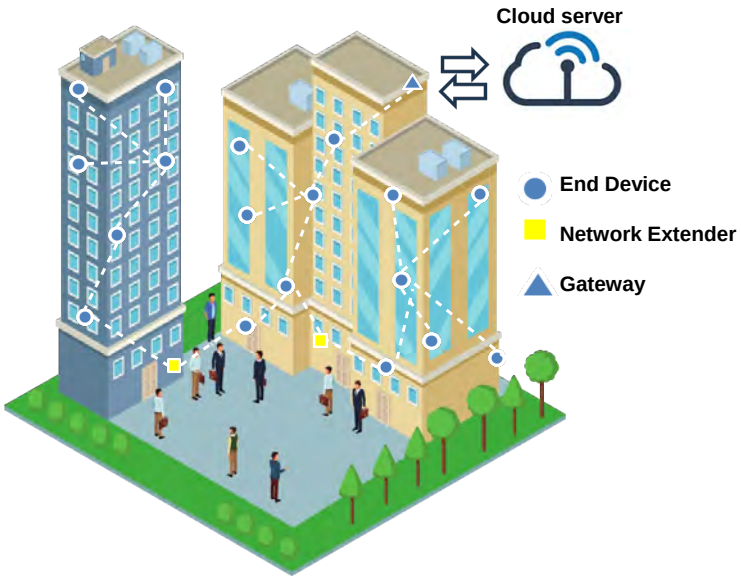


Figure 1.3 LoRa mesh network used the building with different EDs, NEs, and gateways.

LoRa is a unique LPWAN technology known for its extensive coverage, low power consumption, affordability, and robustness to noise, making it a promising solution for IoT applications. These beneficial characteristics primarily stem from the specialized modulation technique used in the LoRa physical layer (PHY) [30]. The Long Range

Wide-Area Network (LoRaWAN) serves as an international standard communication protocol, outlining the Medium Access Control (MAC) and network topology for LoRa wireless networks, which support smart city [31] and environmental monitoring [32]-[34].

However, LoRaWAN primarily supports star topologies and does not provide standards for mesh topologies [34]. This limitation means that extending LoRaWAN coverage typically requires adding more gateways, which may involve additional Internet infrastructure costs. These expenses can be mitigated by utilizing network extenders (NEs) in a mesh network. As shown in Figure 1.3, a mesh network within a building can use various EDs and NEs, all connected to a single gateway. Incorporating NEs is often more cost-effective than installing additional gateways. Furthermore, in many scenarios, connecting new data lines may not be feasible. Overall, mesh networks present a cost-efficient and flexible approach to extending coverage.

Researchers have introduced new MAC protocols for LoRa mesh networks, concentrating on various aspects such as a spreading factor subnet allocation mechanism [35], optimal path routing [36]-[37], and energy efficiency [38]. Data collisions can arise in the absence of an effective collision avoidance (CA) mechanism. Even in single-hop star topologies, the scalability of LoRa-based IoT applications has been a subject of debate among researchers. While there have been significant efforts to enhance the scalability of LoRa star networks to support increased coverage and a larger number of EDs, current research on LoRa MAC protocols has not sufficiently addressed collision management through CA. Additionally, these studies have largely overlooked the distinct collision behaviors encountered in mesh versus star networks. Therefore, Chapter 3 will have the following contributions and objectives:

1. Propose MACs that emphasize collision handling through CA mechanisms, applicable not only to star networks but also to mesh networks.
2. Provide empirical methods for evaluating collision behavior and performance in mesh networks. These methods will be validated to predict long-term performance in large-scale systems. Importantly, they can be conducted in a laboratory setting with a limited number of devices over a short duration.

## 1.3. Proof of concept for stable IoT networks

Building on the improvements made to ensure network stability for IoT systems, Chapter 4 presents a long-term deployment test conducted within a commercial building. In this test, more than 200 devices are connected to a single gateway, spanning 23 contiguous floors in the building's restroom areas over a period of six months. The deployed devices are water flood detection sensors, designed to detect flooding in restrooms without requiring immediate acknowledgment from the property management team.

This deployment test is characterized by its large scale, involving a greater number of devices, wider coverage, and a longer duration compared to previous research efforts. It effectively demonstrates the stability, potential, and feasibility of IoT networks utilizing the proposed MAC protocols and RF filters. Furthermore, this research highlights its significant contribution to society by enhancing water management practices and reducing the risk of property damage, thereby promoting a more efficient and responsive approach to facility maintenance.

# 2. IN-HOUSE INVESTIGATION ON SURFACE ACOUSTIC WAVE (SAW) FILTER DESIGN AND FABRICATION WITH PARAMETRIC VARIATIONS

## 2.1. Introduction

The antenna receives and transmits radio-frequency (RF) signals, both from the wireless device and the surrounding environment. Consequently, it inevitably picks up unwanted signals, including noise and data frames from other wireless technologies. To address this, a filter with a passband specific to the desired wireless solution is employed. The filter effectively removes unwanted signals, ensuring that they do not interfere with the normal operation of the wireless device.

Noise can be effectively rejected by employing properly selected filters. In Chapter 2 of this thesis, we will discuss surface acoustic wave (SAW) filters, which possess several advantageous properties, including low production cost, compact size, and a high quality factor. As the specifications for wireless communication continue to evolve, the design of SAW filters requires ongoing refinement to meet these changing requirements. The remainder of this section presents a comprehensive investigation of filters as follows:

Section 2.2.1: Design Parametric variation of SAW filter

Section 2.2.2: Quick 2D FEM simulation

Section 2.2.3: In-house fabrication in UMF

Section 2.2.4: Measurement and Result

Section 2.2.5: Evaluation of the design parameters

One of the notable achievements of this chapter is the comprehensive simulation, fabrication, and measurement assessment of the SAW filter, all carried out using in-house resources. This entire undertaking was managed on campus by research students, which effectively reduced the time, cost, and labor associated with the design process, thereby advancing the development of SAW filter technology.

## 2.2. Hybrid design approach for 2 port SAW filter

### 2.2.1. Design Parametric variation of SAW filter

| Item | Feature | Variation |
|---|---|---|
| 1 | Presence of reflector | **With**/ Without |
| 2 | Length of IDT overlap | 20/**100**/200 μm |
| 3 | Number of IDTs per port (N) | 10/20/**40**/80 |
| 4 | Number of reflectors per port (M) | 10/20/**40**/80 |
| 5 | Separation of two ports | 100/**200**/400/800 μm |

Table 2.1 IDT Design parametric variations

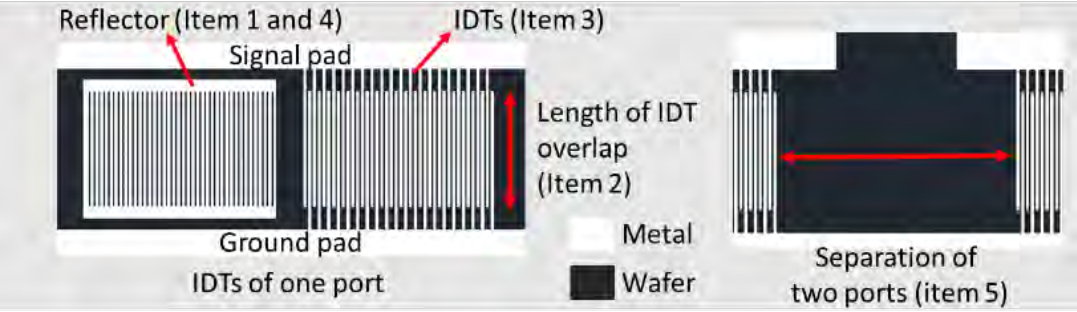


Figure 2.1 IDT parameters overviews

Table 2.1 summarizes the parametric variations of the IDT. The first variation is the presence of reflectors. Reflectors are designed to prevent induced acoustic waves from traveling away from the receiving port. Therefore, filters with reflectors are expected to exhibit lower insertion loss (higher power transmission) than filters without reflectors. The presence of reflectors should not significantly affect the resonance frequency (passband center frequency) or the bandwidth.

The second variation is the overlap length of the IDT finger pairs between the signal and ground pads. Overlap lengths of 20 μm, 100 μm, and 200 μm are selected to demonstrate their effect on filter performance. A longer overlap length is expected to yield better performance, as it provides a larger area for generating and reconverting acoustic waves. However, SAW filters are known for their compact size and low cost. Excessive overlap length increases the wafer area required and ultimately leads to higher cost and a larger device footprint. Therefore, it is important to optimize the IDT overlap length with respect to both size and performance. Although the selected overlap lengths may not be fine enough to determine the exact optimum, they should indicate the approximate range in which the optimal length lies and whether further increases would be beneficial.

The third and fourth variations are the number of IDT finger pairs (N) and the number of reflectors (M) per port. For these variations, 10, 20, 40, and 80 IDT pairs and reflectors are tested to identify an optimal configuration for the filter.

The fifth variation is the port separation. Separations of 100 μm, 200 μm, 400 μm, and 800 μm are tested. All of the above variations are expected to have only a slight effect on the center frequency and bandwidth, and their influence is significantly smaller than that of the pitch. When the pitch size is constrained by fabrication technology, tuning these other design parameters becomes more important. In Table 2.1, the baseline values of the SAW filter parameters are shown in bold, while one parameter at a time is varied. For example, when the IDT overlap length is varied from 20 μm to 200 μm, all SAW filters include reflectors, 40 IDT pairs per port, 40 reflectors per port, and a port separation of 200 μm.

The above design variations will be fabricated on a 128° Y-cut lithium niobate ($LiNbO_3$) wafer. This material is selected because it has a strong piezoelectric coupling

coefficient, allowing efficient conversion and reconversion of surface acoustic waves. The pitch of the filter is not varied, as its effect is clearly described by equation (3). For the following fabrication, a SAW filter with a 2 μm pitch (corresponding to a 4 μm wavelength) will be fabricated. The 2 μm pitch is chosen because it is the finest resolution supported by the UMF facilities.

### 2.2.2. Quick 2D FEM simulation COMSOL Multiphysics for resonance frequency prediction.

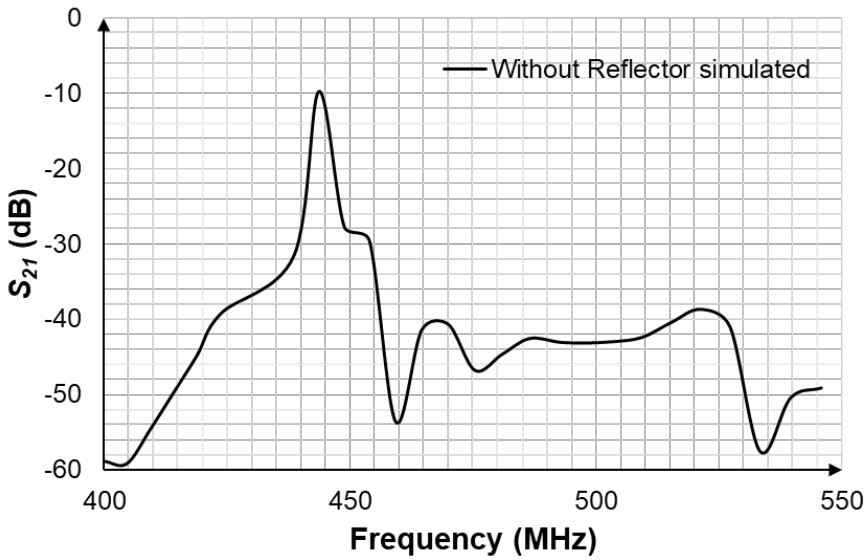


Figure 2.2 Simulated frequency response for 2μm pitch SAW filter without reflector

As mentioned in the literature review section, 3D FEM simulation can capture most of the details but incurs a high time cost, even on high-end computers; therefore, a reduced 2D simulation is used instead. The 2D simulation ignores the detailed IDT design and only aims to provide a rough resonance-frequency prediction.

COMSOL Multiphysics, a commercially available FEM simulation software, is used to conduct the 2D simulation. A two-port SAW filter on lithium niobate with 20 pairs of IDTs on each port and no reflectors is simulated. The result is shown in Figure 2.2.

The resonance is located at around 440 MHz with −10 dB insertion loss and a 5 MHz bandwidth. This result is relatively rough, as only a quick 2D simulation is conducted instead of a full 3D simulation. The simulation is completed within minutes on a computer with an Intel i5 2.4 GHz CPU and 4 GB of RAM, which is a common configuration for daily office work. The computational time is drastically reduced at the expense of accuracy. Therefore, fabrication and measurement are essential to complement and validate the simulation results.

### 2.2.3. In-house fabrication in UMF.

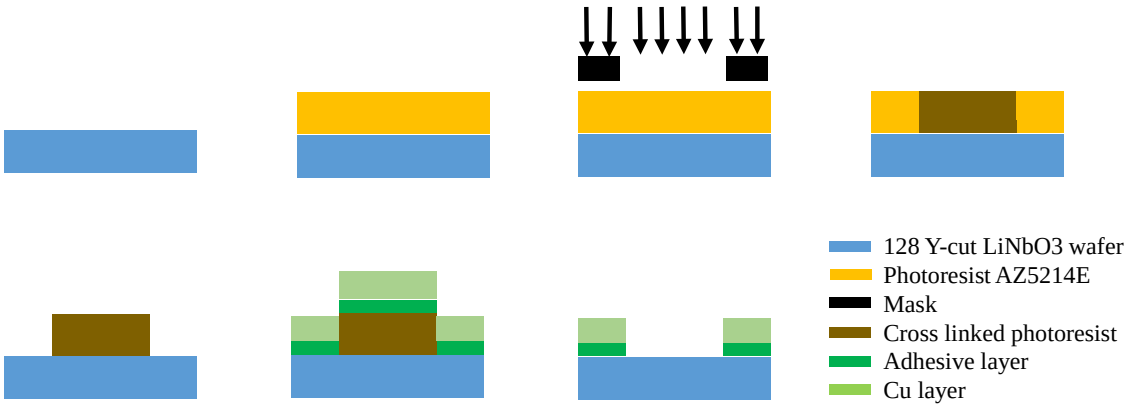


Figure 2.3 In-house fabrication process of SAW filter

All SAW filter fabrication procedures are carried out at The Hong Kong Polytechnic University's University Research Facility in Materials Characterization and Device Fabrication (UMF), except for the mask fabrication. Figure 2.3 shows the fabrication procedure of the SAW device.

First, the lithium niobate wafer is cleaned and spin-coated at 3000 rpm using the Sawatec spin coater to form a uniformly distributed layer of AZ5214E photoresist. The coated wafer is then transferred to the SUSS MA6 mask aligner. The mask aligner is equipped with a mask containing the designed IDT pattern. Next, the wafer is mounted onto the mask aligner and brought into soft contact with the mask. The photoresist on the wafer is exposed to UV light and becomes cross-linked. Some areas of the

photoresist are shielded by the mask, so no cross-linking occurs there. After UV exposure, the coated wafer is rinsed in the developer; the cross-linked photoresist remains on the wafer surface, while the unexposed photoresist is removed. In this way, the mask pattern is transferred to the wafer.

The patterned wafer is then transferred to the Denton Explorer 14 sputtering system. A copper layer is deposited onto both the exposed wafer surface and the remaining photoresist. Finally, the deposited wafer is rinsed in acetone. The cross-linked photoresist is removed, and the metal on top of it is lifted off. As a result, a wafer with the metallic IDT pattern is obtained.

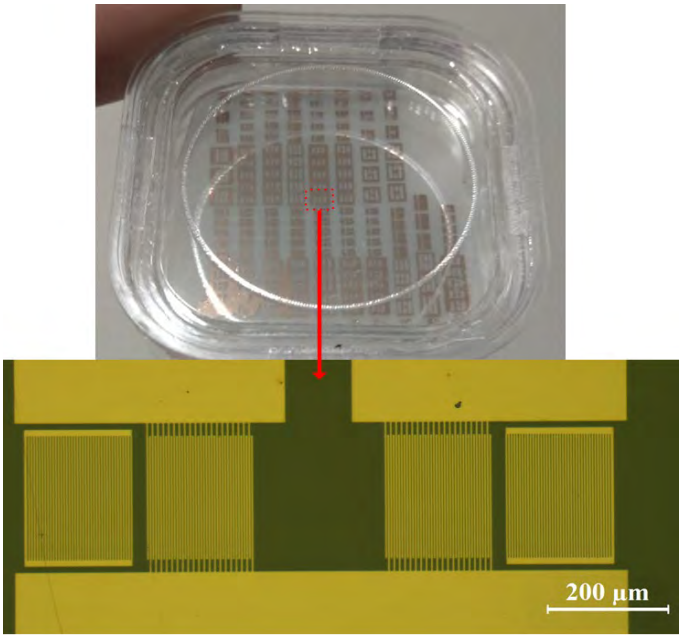


Figure 2.4 In-house fabrication process of SAW filter

One of the fabricated wafers is shown in Figure 2.4. More than 100 SAW filters can be fabricated within one 3 cm × 3 cm wafer. For ease of landing the probes, dedicated signal and extra ground pads are designed. In real applications, smaller pads could be used so that even more and denser SAW filters could fit on the same wafer. All the IDT design patterns from items 1 to 5 in Table 2.1 are fabricated onto one wafer, and each pattern has around five copies, so that generally there will be at least one

successfully fabricated pattern for each IDT design.

The fabrication process listed in Figure 2.4 can be completed within one day, and all 17 parametrically varied IDT designs are fabricated. On the other hand, if design verification relies mainly on 3D simulation, the simulation must include most fine details, and it will take nearly two months to finish with a high-end hardware configuration [9]. Therefore, in this work, an oversimplified, quick 2D simulation with lower accuracy is used to estimate the resonance frequency, and then the resonance frequency and frequency response are verified by actual fabrication and measurement. In this way, one cycle of the design process can be shortened to a few days.

### 2.2.4. Measurement and result.

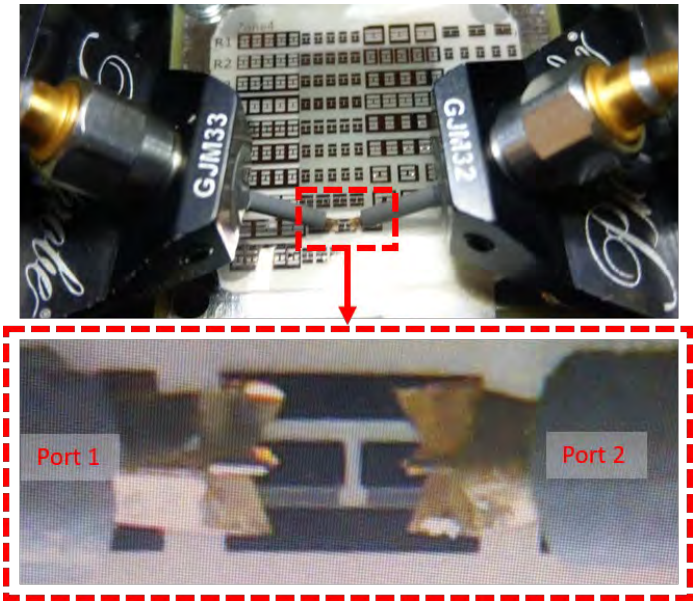


Figure 2.5 Photograph of probe station frequency response measurement

Figure. 2.5 shows the probe station frequency response measurement of the filters. The wafer with filters is placed onto a handling platform. The two ground-signal-ground (GSG) probes carefully land onto the fabricated SAW filter's signal and ground pads. Another end of probes is connector the port one and port two of the vector network analyzer (VNA) so that the S-parameters ($S_{11}$ and $S_{21}$) could be measured. $S_{11}$ represents the ratio of input power in port one over the reflected power in port one in dB scale. $S_{21}$

represents the ratio of input power in port one over the received power on port two in dB scale. When the measured frequency is outside the passband, the ideal filter's $S_{11}$ should be close to 0dB and $S_{21}$ should be as small as possible, which indicates most of the power is reflected from port one and not received by port two. On the other hand, when measured frequency is inside the passband, ideal filter's $S_{11}$ should be as small as possible and $S_{21}$ close to 0dB, which indicates most of the power converted in port one and received in port two.

### 2.2.5. Evaluation of the design parameters.

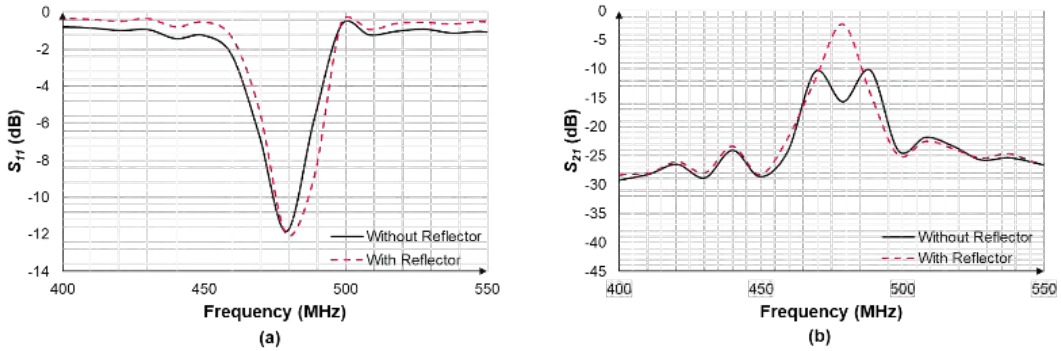


Figure 2.6 Frequency response comparison of (a) reflection coefficient ($S_{11}$) and (b) transmission coefficient ($S_{21}$) with reflector's variations

Figure 2.6 shows the impact of the presence of the reflector. From Figure 2.7(a), $S_{11}$ for filter with reflector and reflector are similar. At around 480MHz, both filters have $S_{11}$ better than -10dB, which indicates electrical power is effectively converted in port one. From Figure 2.7(b), the $S_{21}$ for filter with reflector is significantly better than filter without reflector. The filter with reflector could have the best $S_{21}$ of -3dB but the one without could only have the best $S_{21}$ of -10dB. By examining both graphs, we can conclude that the electrical signal is successively converted into an acoustic wave in both designs. However, in the absence of the reflector, the acoustic wave is not efficiently directed to the second port, leading to significant power loss and a reduced transmission coefficient.

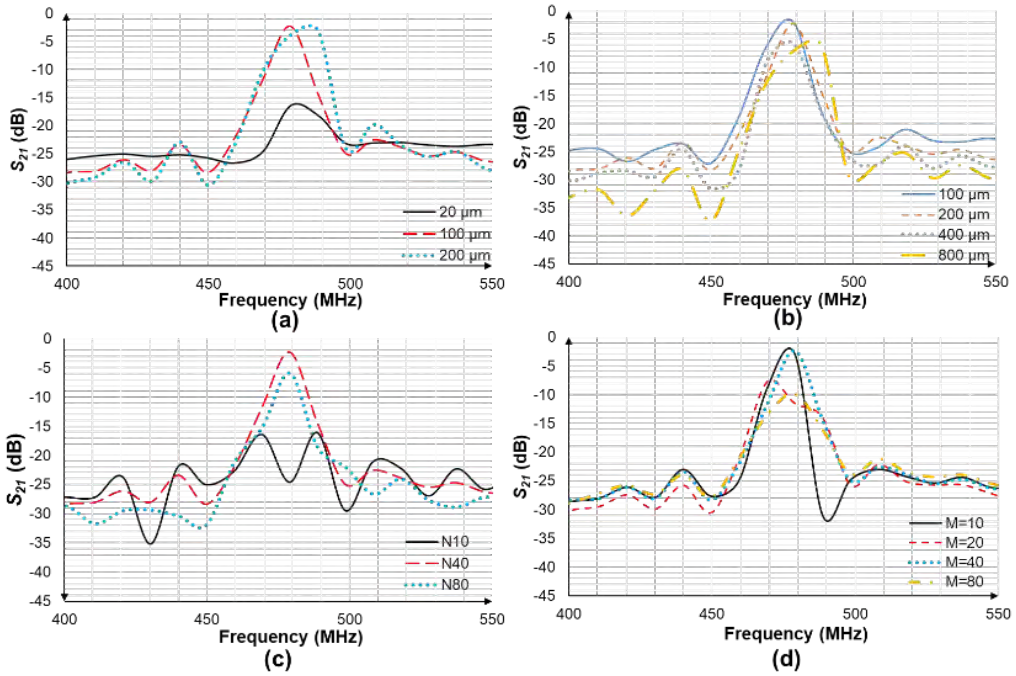


Figure 2.7 Comparison of transmission coefficient ($S_{21}$) with variations of (a) length of IDT overlap, (b) separation of two ports, (c) number of IDTs per port and (d) number of reflectors per port.

For the rest of variations, only $S_{21}$ is measured as reflector is present, the capability of converting electrical wave and reconverting acoustic in both ports should be the same.

For the length of IDT overlaps in Figure 2.7 (a), 20µm, 100µm d 200µm are measured. The filter with only 20µm IDT overlap is not sufficient generating and reconverting acoustic wave, so that it's best $S_{21}$ is only at -15dB. 100µm and 200µm have a similar performance of the best $S_{21}$ of -3dB. The 100µm filter has around 15MHz bandwidth better than -10dB and 200µm filter has around 20MHz bandwidth. From power transmission perspective, increasing IDT overlapping length brings no benefit but increasing the size and cost. Finer steps for IDT overlap length should be taken from 20µm to 100µm to find out the optimal size with the best $S_{21}$ of -3dB. If a broader band filter is desired, a longer IDT overlap could help. Finer steps and a broader step range should be done to further confirm this observation.

For port separation, 100µm, 200µm, 400µm and 800µm are fabricated and

measured. From Figure 2.7 (b), we could observe that the best $S_{21}$ is decreasing with increasing port separation, and the band rejection out of passband is increasing with increasing port separation. Larger port separation indicating longer space the acoustic wave should travel, so that the attenuation increases. At the same time, we could observe the center resonance frequency is slightly drifted from left to right in frequency domain with increasing port separation, which could be used to slightly manipulate the resonance peak by introducing more attenuation.

For number of IDT pairs per port (N), 10, 40, and 80 pairs of IDT are compared. From Figure 2.7 (c), 10 pairs of IDT are not sufficient to effectively convert and reconvert the acoustic wave that only the best $S_{21}$ of around -15dB could be observed. Interestingly the best $S_{21}$ do not approach to 0dB from increase 40 pairs to 80 pairs per port. The best $S_{21}$ decrease from -3dB to -5dB by increasing 40 pairs to 80 pairs. It is perhaps due to the longer travelling distance hence attenuation with more IDT pairs. This observation should be further investigated with fine steps between 40 and 80 pairs.

Finally, from Figure 2.7 (d), we could observe the best $S_{21}$ do not improve with increasing reflector numbers from 10 to 80 pairs per port, indicating few reflectors are sufficient to reflect the acoustic wave. It is recommended to limit the reflector number to save wafer area and cost. The data of 20 and 80 pairs of reflectors are off the trend. It may be due to poor fabrication as these two variation is located at the margin of the wafer.

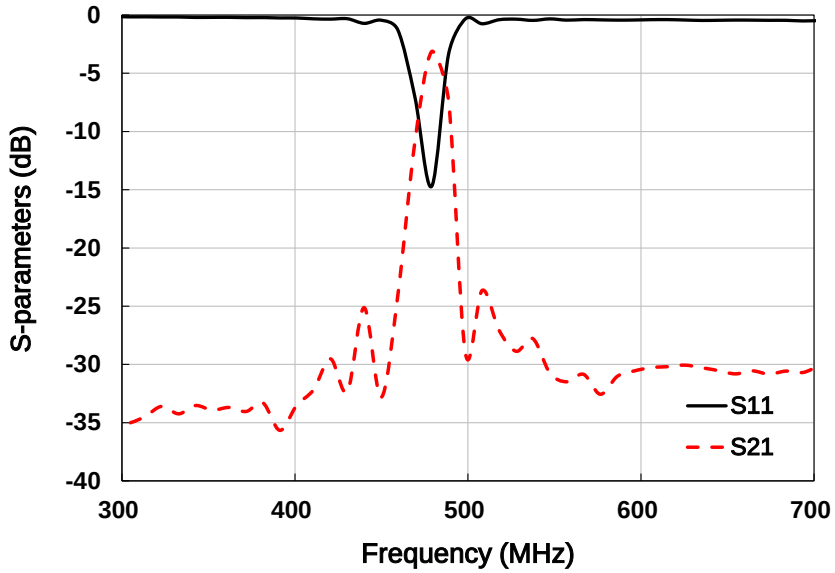


Figure 2.8 *S*-parameters ($S_{11}$ and $S_{21}$) of best fabricated filter at 480 MHz

The best fabricated SAW filter is shown in Figure 2.8, which has 100μm IDT overlap length, 100μm port separation, 40 pairs of IDT and reflector per port. This filter has the best $S_{21}$ of -3dB and best $S_{11}$ of -15dB. Its resonance frequency center at around 480MHz with a bandwidth around 15MHz above -10dB. This passband frequency range is located within the LoRaWAN band CN470-510.

## 2.3. Section Summary

In this chapter, a complete SAW filter design workflow is demonstrated, and the effects of parametric variations are examined. The most significant outcome of this research is the establishment of a rapid, fully in-house procedure covering design, simulation, fabrication, and measurement within a short development cycle. Although the study includes several parametric variations, such as the IDT overlap lengths of 20, 100, and 200 μm in the previous section, these steps are relatively coarse. Finer and broader variations in overlap length could be explored, as the selected values may not be sufficient to identify the true optimal design. Nevertheless, they are adequate for

demonstrating the full workflow and validating the methodology.

Second, during the design process, a simplified 2D FEM approach was combined with fabrication and measurement instead of relying solely on accurate but time-consuming 3D FEM simulations. For 17 parametric variations, the time required was reduced from nearly two months to just a few days. Moreover, the measurement results represent the actual device behavior and are therefore ultimately more reliable than even high-fidelity 3D FEM predictions.

Furthermore, the impact of each IDT design parameter was evaluated. Reflectors are necessary for realizing a low loss SAW filter; however, an excessive number of reflector fingers provides no additional benefit and only increases the device size and cost. An IDT with 40 finger pairs and a 100 μm overlap is sufficient: further increasing the overlap length may broaden the bandwidth but does not improve the transmission coefficient. The resonance frequency can also be slightly shifted by increasing the port separation. These observations, however, should be further verified using both broader ranges and finer steps in the parametric variations.

In addition, a 480 MHz bandpass filter suitable for the LoRa CN470–510 band was fabricated during this work, demonstrating the potential of low-cost SAW filters for IoT applications.

Finally, Hong Kong currently has no large-scale semiconductor manufacturing industry and only a few semiconductor and RF component design houses. The Hong Kong Polytechnic University is one of the organizations with the capability to design and fabricate such components in-house. This work therefore highlights an opportunity for closer collaboration between the University and the local electronics design industry.

# 3. EMPIRICAL INVESTIGATION OF MEDIUM ACCESS CONTROL WITH EFFICIENT MEDIUM UTILIZATION FOR LORA IOT APPLICATIONS

## 3.1. Introduction

In Chapter 2, we explored the stability of IoT networks at the level of electronic circuit components. One of the key components, the SAW filter, plays a crucial role in enhancing the resilience of RF circuits against environmental noise. In Chapter 3, we will expand our focus from the circuit level to the system level, examining how multiple end devices can lead to instability and how to avoid these issues.

Filters can effectively reject noise or signals that fall outside the operational frequency range of the wireless device. The filtered incoming analog signal is then amplified and demodulated by the transceiver into a digital signal, which is forwarded to the baseband processor. The baseband processor, a type of microcontroller unit (MCU), manages medium access by determining when to transmit, receive, or back off. This unit also performs collision avoidance to ensure efficient communication. However, sources of instability may still exist within this frequency range. When multiple devices transmit concurrently on the same frequency channel, collisions can occur. Therefore, an efficient medium access control (MAC) strategy is essential for forming a stable IoT network.

In Chapter 3 of this thesis, Long Range (LoRa), a promising existing IoT solution, is selected for further exploration. This chapter focuses on improving the MAC layer

of LoRa by expanding its original star network topology into a mesh network. This enhancement addresses the challenge of contention when multiple devices attempt to transmit simultaneously without centralized coordination. By implementing the proposed MAC in a mesh network structure, the system can better manage communications and reduce the likelihood of collisions, ultimately leading to a more reliable and scalable IoT network.

### 3.1.1. LoRa Physical Layer (PHY)

According to OSI seven-layer model, LoRa is located in the Physical Layer (PHY) that governs how the LoRa radio wave should carry and transmit the bits from one transceiver to another. The LoRa modulation utilizes the chirp spread spectrum (CSS) with forward error correction (FEC) to achieve robust long-distance communication. The key features of the LoRa PHY could be explained by spread spectrum, chirp, and error coding.

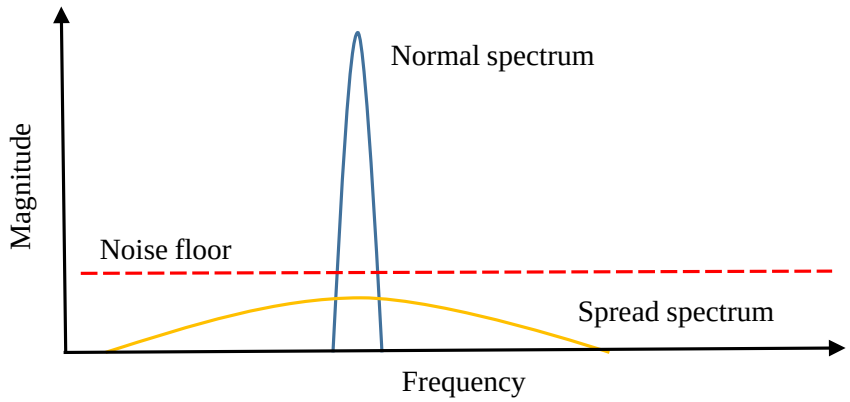


Figure 3.1 The comparison of spread spectrum and normal spectrum.

In spread-spectrum systems, the signal is further expanded beyond its original bandwidth without increasing its total energy, which means the energy is spread over the frequency domain instead of being concentrated in a narrow frequency band. The spreading is performed by the transmitter according to a predefined code sequence and

is reversed by the receiver. This spreading procedure provides additional processing gain, allowing the receiver to recover the original signal even when the modulated signal is below the noise floor, as shown in the extreme case in Figure 3.1.

Even when there is a high noise floor within the same frequency band, implying that many wireless devices are already using that band, the LoRa signal can still be spread over the band to levels lower than the noise floor and yet be successfully demodulated. Therefore, LoRa can more easily operate reliably in channels shared with other wireless applications.

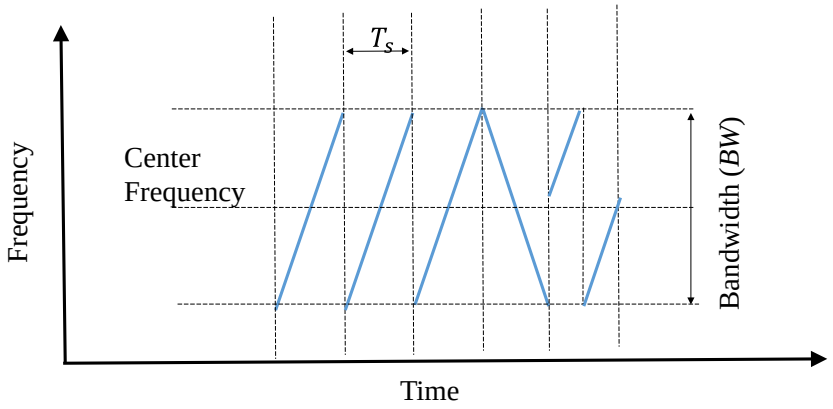


Figure 3.2 Example of LoRa PHY chirp sweeping.

Figure 3.2 shows an example of LoRa chirp sweeping in the time domain. This example consists of 3 up chirps, 1 down chirp and a symbol. The speed-related parameters, such as bandwidth (*BW*) and symbol time ($T_s$), and LoRa PHY packet structure after converting into byte field will be discussed in the following session.

A chirp is a frequency-sweeping process bounded by the spread bandwidth. An up-chirp sweeps from low to high frequency, while a down-chirp sweeps from high to low frequency. From a physical perspective, each chirp contains a predefined number of chips, which corresponds to the number of frequency-sweeping steps. Each chirp carries one symbol, and each symbol contains a predefined number of bits, which does not necessarily have to be 8 bits. The bits within the symbol include not only the raw

data bits but also the FEC bits. The FEC bits help the receiver recover the original data even when a certain number of bits are corrupted.

The LoRa modulation process includes adding FEC bits into original data, chirp formation by translating processed bits into symbols and chirp spectrum spreading bounded by *BW*. In such a process, coding rate (*CR*) for FEC, spread factor (*SF*), and *BW* influence the bit rate ($R_b$) in bits per second (bps), and these parameters are configurable.

The *CR* ranged from 1 to 4, defines cyclic coding rate, the ratio between raw data bits and total bits including the redundant FEC bits. For example, for *CR* = 1, every 5 sent bit contains 4 raw data bits, for *CR* = 2, every 6 bit contains 4 raw data bits, etc. The examples of *CR* and cyclic coding rate are listed on Table 3.1. The more FEC bits are added, the more resistance to the noise is. However, the effective $R_b$ decreased due to the presence of redundant bits.

| Coding Rate (*CR*) | Cyclic Coding Rate |
|---|---|
| 1 | 4/5 |
| 2 | 4/6 |
| 3 | 4/7 |
| 4 | 4/8 |

Table 3.1 Coding Rate (*CR*) to Cyclic Coding Rate conversion

The *SF* and *BW* need to be explained together in the physical sense. The *SF* ranged from 6 to 12 indicates the total number of bits carried by one symbol. The bits here include both raw data bits and FEC bits. Also, the total number of chips within a chirp symbol could be calculated by $2^{SF}$. The *BW* defines not only the distance between the upper and lower bounds of frequency sweeping but also the chip rate. In the LoRa PHY contest, *BW* has the unit of chips per second. The symbol $T_s$ could be calculated by

equation (3.1).

$$T_S = 2^{SF} / BW \tag{3.1}$$

The larger *BW* and smaller *SF* reduce the Time on Air (*ToA*) of transmitting a symbol. However, the larger *BW* means the chip changes more rapidly and smaller *SF* means the total amount of chips is reduced that makes successful demodulation in the receiver side more difficult. Therefore, a larger minimum signal to noise ratio (SNR) is required to conduct successful demodulation.

Combining the effect of *CR*, *SF*, and *BW*, the effective $R_b$ could be calculated according to equation (3.2).

$$R_b = SF\left(\frac{BW}{2^{SF}}\right)\left(\frac{4}{4+CR}\right) \tag{3.2}$$

Table 3.2 illustrates how these parameters alter the $R_b$ and the minimum reception SNR requirement [20].

| Configuration | | | Theoretical performance | |
|---|---|---|---|---|
| *SF* | *BW* (kHz) | *CR* | Minimum SNR (dB) | Bit Rate ($R_b$) (bps) |
| 7 | 500 | 4 | -117 | 13672 |
| 12 | 500 | 4 | -117 | 732 |
| 7 | 125 | 4 | -131 | 3418 |
| 7 | 500 | 4 | -137 | 21875 |
| 12 | 125 | 1 | -117 | 293 |
| 12 | 125 | 1 | -137 | 183 |

Table 3.2 Theoretical performance under different configuration

Figure 3.3 shows the LoRa packet structure. The LoRa packet comprises of four parts, a preamble, an optional header, an actual data payload which consists of the raw bits and FEC bits, and an optional 16 bits payload CRC could be added. The preamble includes a configurable number of up-chirps and 4.25 compulsory chirps, followed by 2.25 down chirps. The preamble is used to indicate the beginning of a packet. The

second component of the packet is the header, which includes the information on the payload length, the presence of the payload CRC, and the *CR* of the payload. Payload is placed after the header, which contains the actual data. If payload CRC is enabled in the header, payload CRC will be appended at the end in the packet. All configurable parameters, including *SF*, *BW*, *CR*, preamble length, presence of header, and 16 bits payload CRC should be identical for both sides of transmission and reception to have successful demodulation.


Figure 3.3 LoRa PHY packet structure.

Theoretical $R_b$ is calculated by selecting SF, *BW*, and *CR*. In the practical case, packet loss should be considered. Packet loss could be due to packet corruption in long-range transmission and packet collision. The first case is well-addressed by LoRa modulation. However, the second case is not specified by LoRa PHY. Packet collision occurs when two data packets occupy the air medium with the same center frequency, *BW* and *SF*, resulting in the loss of both packets. If two packets with different *SF*s are sent simultaneously, both packets are possible to be successfully demodulated as they are orthogonal to each other, even if the orthogonality is not perfect. Also, if there is significant signal strength difference between two packets, the stronger one could survive successful demodulation.

### 3.1.2. Medium Access Control (MAC) Layer

The data link layer is the next layer on top of the PHY layer, which was discussed in the previous subsection. The data link layer is further divided into two sublayers: the logical link control (LLC) layer and the medium access control (MAC) layer. Neither

sublayer is defined by the LoRa PHY specification. However, they are necessary for efficient wireless communication, especially the MAC layer, which governs how the medium is accessed. An inadequate MAC layer specification can lead to data collisions, which may drastically reduce the practical bit rate compared to the maximum theoretical bit rate

LoRa Alliance proposed LoRaWAN protocol for LoRa public application [34]. LoRaWAN is built on top of LoRa, and the LLC and MAC sublayers are further defined. LoRa modulation alone does not necessarily fulfill the LoRaWAN specification. However, the LoRaWAN protocol must conform to the LoRa PHY specification. Therefore, it is possible to implement a custom private protocol for LoRa-based applications.

In the LoRaWAN specification, devices are categorized into three classes: Class A, Class B, and Class C, where the end devices (EDs) are suited to applications with decreasing battery life expectations from Class A to Class C. These classes primarily focus on optimizing battery life by controlling the sleep interval, sleep duration, and wake duration. All classes of EDs utilize the pure ALOHA protocol for medium access control (MAC) [34]. This primitive MAC is used by LoRaWAN as it is designed for low duty cycle applications.

#### *3.1.2.1 Pure ALOHA (P-ALOHA)*

LoRaWAN utilizes Pure ALOHA (P-ALOHA) as its basic MAC protocol, which allows end devices (EDs) to transmit packets at any time without considering the state of the medium. However, this can lead to collisions when packets overlap in time and frequency.

In LoRaWAN, EDs are designed to operate under a low-duty cycle, constrained by regional frequency-band regulations. For instance, in Hong Kong (AS923 in the ISM

band), the duty cycle is limited to less than 1 % [39]. As a result, EDs spend most of their time in deep sleep mode, transmitting only short frames when necessary. Under these conditions, without CA may not be significant to successful transmissions.

Researchers investigating the scalability of LoRaWAN have developed models to analyze the performance of single-gateway LoRaWAN system [40]. The successful transmission's probability exponentially decays with an increase in the number of Eds [41]. This decline is primarily attributed to interference that arises when multiple EDs transmit simultaneously using the same frequency and SF. Satisfactory scalability can only be achieved by restricting the amount of data each device transmits in a single day. This low traffic and the resulting delays confine LoRaWAN to non-critical monitoring applications [42]. These limitations significantly diminish service providers' interest in deploying LoRaWAN-based monitoring systems. Consequently, managing collisions is crucial for enhancing the capabilities of LoRa in various applications.

#### *3.1.2.2 Slotted ALOHA (S-ALOHA)*

The Slotted ALOHA (S-ALOHA) protocol is an extension of the Pure ALOHA (P-ALOHA) protocol. In an S-ALOHA network, end devices (EDs) begin their transmissions only at the start of designated time slots. Despite this structured approach, collisions can still occur if multiple EDs attempt to transmit during the same time slot. In theory, S-ALOHA offers better performance than P-ALOHA and is considered a viable alternative to address the significant limitations of P-ALOHA in LoRaWAN. Numerous studies have been conducted to evaluate the performance of S-ALOHA and explore its integration into the LoRa MAC layer [43]-[45].

A practical air sensor network was developed using an S-ALOHA overlay on LoRaWAN [43]. Under heavily loaded traffic conditions, channel throughput improved

from 2.6% to 15% when transitioning from P-ALOHA to S-ALOHA. This increase in throughput was due to an improvement in the packet delivery ratio (PDR), which rose from 7% to 33%. The study demonstrated that S-ALOHA enhances the likelihood of successful transmissions by reducing collision probability. Instead of relying on simulations with multiple EDs operating at a low duty cycle (below 1%), the authors implemented a heavily loaded scenario with one gateway and 24 actual EDs actively transmitting packets. This heavily loaded configuration serves as the basis for current research, which also uses a limited number of devices.

Instead of relying on random slot access, a research group proposed using a 64-bit MAC address, which serves as a unique device ID assigned by the manufacturer, to allocate slots to devices in S-ALOHA [44]. In their experiment, 10 EDs achieved a PDR of nearly 100% when using 28 slots at SF7 with S-ALOHA. In contrast, P-ALOHA only reached about 60% PDR under the same conditions. This research further validated the advantages of S-ALOHA in providing a more effective MAC protocol. Additionally, the study introduced a straightforward method for assigning slots to EDs, which helps prevent multiple devices from randomly accessing the same slot—a key limitation of traditional S-ALOHA.

A previous study expanded the analysis of P-ALOHA and S-ALOHA from fixed packet lengths to variable packet lengths, providing a more accurate reflection of real-world applications [45]. The authors presented analytical results highlighting two opposing effects of S-ALOHA. While it protects ongoing transmissions from collisions, it fails to efficiently utilize idle channel time if the time slot is configured for the maximum packet size. Conversely, if the time slot is shorter than the packet duration, the throughput of S-ALOHA can be lower than that of P-ALOHA.

In summary, earlier studies on S-ALOHA have demonstrated that slotting can safeguard ongoing transmissions under heavily loaded conditions. Replacing randomly

selected slots with ID-allocated slots has been shown to enhance the PDR. However, the challenges posed by variable packet lengths must also be addressed. Consequently, S-ALOHA is used as a reference in this study for addressing collision issues associated with LoRa in mesh applications..

#### *3.1.2.3 Carrier-Sense Multiple Access CSMA/CA*

Researchers have explored Carrier-Sense Multiple Access (CSMA)-type MAC protocols for LoRa applications, notably CSMA with Collision Avoidance (CSMA/CA), as implemented in the IEEE 802.11 standard for Wi-Fi networks. This protocol employs Listen-Before-Talk (LBT) strategies within star-topology networks. Before an ED transmits data, it first checks the medium's occupancy during the Distributed Interframe Space (DIFS). If the medium is detected as idle for the entire DIFS period, the ED proceeds with transmission. If the medium is occupied, the ED delays its transmission until the ongoing transmission concludes.

Afterward, the ED senses the medium again for another idle DIFS period, adding a random backoff time slot within the range [0, CW − 1], where CW represents the contention window. This backoff strategy is termed exponential backoff, as CW doubles with each retry until it reaches a predetermined maximum. The backoff timer decreases when the medium is idle but pauses when the medium is occupied. It resumes counting down once the medium becomes idle again, and transmission occurs when the timer reaches zero.

Researchers have adapted CSMA/CA for LoRa networks, demonstrating stable, long-range data transmission through a Carrier Access (CA) mechanism in both experiments [46] and simulations [47]. The proposed method utilized the Channel Activity Detection (CAD) procedure for medium sensing and implemented the LBT strategy. The study's findings indicated that the CAD procedure could successfully

detect not only the LoRa PHY preamble but also the payload. However, instances of false idle detection were also observed. To address this, the researchers recommended using nine consecutive CAD procedures to fulfill the role of DIFS, as used in IEEE 802.11.

In scenarios where the medium was sensed as occupied, a simple delay equal to the maximum packet duration was applied instead of continuous sensing, which helped mitigate false idle detection. Although this adaptation resulted in longer latency compared to the original IEEE 802.11, it successfully enabled collision-free transmission of long packets.

The performance of P-ALOHA-based LoRaWAN and CSMA-based LoRa networks was investigated and compared through simulation [48]. In this study, a maximum of 10,000 EDs with a low duty cycle of 1% and 10-byte short packets were simulated. The results showed that, with 10,000 EDs, the PDR of LoRaWAN was below 20%, while the PDR of the CSMA-based LoRa network remained above 60%. These findings indicate that CSMA is a significantly more effective MAC protocol for channel access in networks with a large number of EDs compared to P-ALOHA.

A group of researchers conducted a comprehensive comparison of P-ALOHA-based, S-ALOHA-based, and CSMA-based LoRa networks [49]. The results demonstrated that CSMA is not only a more reliable MAC protocol but also more energy-efficient than S-ALOHA, particularly in scenarios where devices are in proximity and transmissions use small SFs.

The research outlined in the above section focused on minimizing collisions among EDs within various MAC protocols in LoRa star networks. However, it is important to note that there is a second type of collision that has received less attention in the past literature, specifically collisions among NEs in mesh networks. In this section, we explore the intrinsic differences between collisions among EDs in star

networks and collisions among NEs in mesh networks.

### 3.1.3. Collisions among End Devices

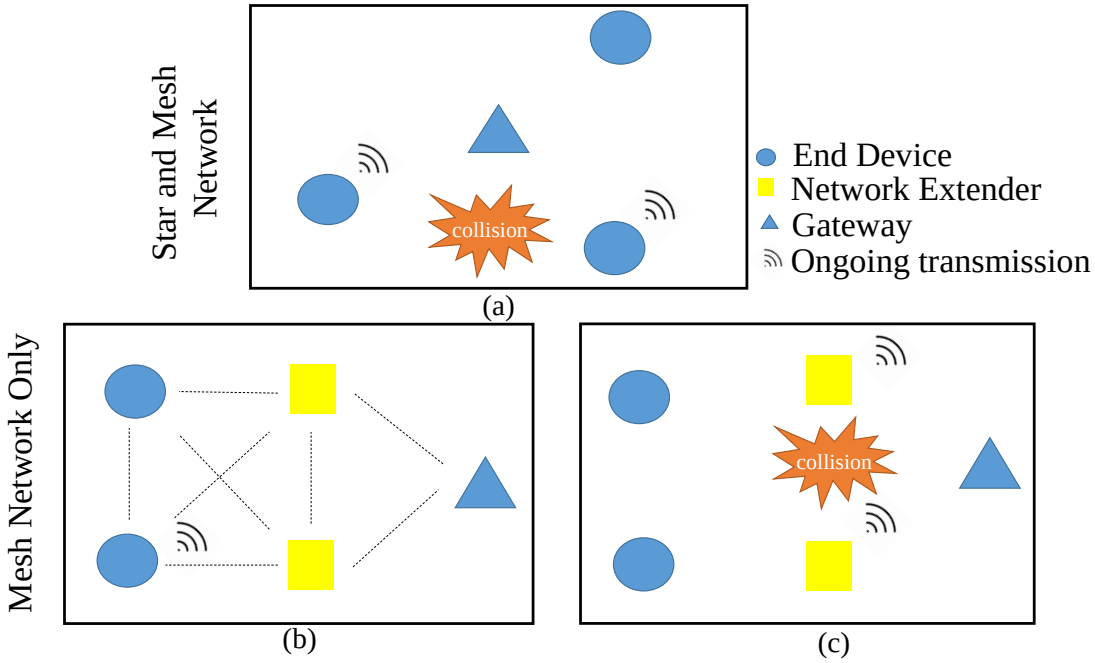


Figure 3.4 Collision behavior of mesh and star networks: (a) collision in both star and mesh networks by EDs, (b) transmission in mesh network by a single ED, and (c) collision in a mesh network by NEs.

The first type of collision arises from transmissions by independent EDs. Figure 3.4(a) illustrates a basic star network comprising one gateway and three EDs. Typically, EDs gather data from sensors through wired connections, while the gateway wirelessly receives data packets from each ED. Each ED begins its transmission based on its own conditions, such as changes in sensor status or the need to send a heartbeat packet to maintain the connection. The transmission initiation of one ED does not influence that of another, making their transmission events independent.

In smaller systems, simultaneous transmissions are rare, but the likelihood of such collisions increases as the number of devices grows. Most existing studies on collisions and scalability in LoRa star networks have focused on this type of collision by

simulating or constructing very large systems with numerous EDs, effectively addressing scalability issues among EDs in star networks. However, they often fail to consider collisions among Network Elements (NEs) in mesh networks.

### 3.1.4. Collisions among Network Extenders

The second type of collision occurs among NEs and does not result from independent events, but rather from recent transmissions by EDs. Figures 3.5(b) and 3.5(c) illustrate two instances within the same mesh network, which includes one gateway, two NEs, and two EDs. The dashed lines indicate the coverage areas of each component in the mesh network. The roles of the gateway and EDs remain the same as described in Subsection 3.3.1, while the NE serves a special function as an ED that forwards packets from other EDs to the gateway.

In the first instance, shown in Figure 3.5(b), one ED initiates a transmission that can reach the other ED and both NEs, but not the gateway directly. In the subsequent moment, depicted in Figure 3.5(c), both NEs attempt to forward the received packet to the gateway simultaneously, resulting in a collision. Consequently, a contention period arises after each ED transmission. This type of collision is likely to occur even in a small mesh network, as illustrated in Figures 3.5(b) and 3.5(c).

In other research, collisions are avoided by assigning different SFs to various EDs and NEs[35],[38],[50]. By utilizing different SFs, the packets become nearly orthogonal, preventing collisions even when they are transmitted simultaneously. This SF allocation effectively decreases the number of NEs and EDs competing for the same channel at any given time. However, as the number of NEs and EDs with the same SF in a specific area increases, collisions among NEs are still likely to occur.

Another strategy involves optimal pathfinding from EDs to gateways through Nes [36] [51]. In this method, each NE forwards only the packets from its designated EDs, which helps minimize excessive packet forwarding. However, obstacles or moving

objects can occasionally obstruct the optimal path. To enhance the reliability of a mesh network, it is beneficial to include at least one redundant path. Despite these mitigations, any remaining collisions among NEs must still be addressed.

The methods mentioned above primarily target the first type of collision. However, there has been limited investigation into how effectively existing MAC protocols manage the second type of collision, which arises not from independent events but from recent transmissions by EDs. Therefore, in Section 3.2 of this chapter, a MAC protocol tailored for mesh networks is proposed to reduce the frequency of collisions among NEs.

Additionally, due to the inherent differences between the two collision types, a novel approach for collision analysis is introduced in Section 3.3. While previous studies typically involved several EDs sending packets randomly and recording their PDRs, this research focuses on collisions among NEs by having each ED periodically transmit packets that NEs then forward. The PDR of the NEs is subsequently recorded. Details of the experimental setup are discussed in Section 3.4.

Although this study is not the only one examining LoRa mesh networks, it is among the few that specifically address collisions among NEs.

## 3.2. Development of MAC for Mesh Network

IIn this section, we propose Carrier Sense Multiple Access (CSMA) methods and test various combinations of these methods for comparative analysis. We gradually incorporate MAC features into the test cases to demonstrate how these enhancements improve the Packet Delivery Ratio (PDR) by reducing collisions. The rationale behind each design choice is also explained to clarify their effectiveness.

A total of six MAC approaches were tested in the experiments. The first two

approaches serve as reference cases, while the remaining four are the proposed approaches. The differences and features of the six MAC protocols are listed in Table 3.3 and Table 3.4. All odd-numbered cases are configured without CAD, whereas all even-numbered cases include CAD. For simplicity, the six MAC approaches are referred to by case number in the following sections. A brief summary of the reference and proposed MACs is provided in Table 3.4, and the details of each MAC approach will be discussed in the following.

| | **Immediate (reference)** | **Slotted delay Rely on random number $N_r$** | **Slotted delay Rely on assigned number $N_s$** |
|---|---|---|---|
| **Without CAD** | Case 1 | Case 3 | Case 5 |
| **With CAD** | Case 2 | Case 4 | Case 6 |

Table 3.3 MAC Strategy principle of each cases

| **Case** | **Strategy** |
|---|---|
| 1 | Transmit immediately regardless of the channel condition |
| 2 | Transmit after two CAD procedures with free channel detected |
| 3 | Transmit after blocking for $T_{slot} * N_r$ |
| 4 | Transmit after $2*N_r$ CAD procedures with free channel detected |
| 5 | Transmit after blocking for $T_{slot}*N_s$, then respond |
| 6 | Transmit after $2*N_s$ CAD procedures with free channel detected |

Table 3.4 Backoff strategy used in each cases

Case 1 is a reference representing the condition without any actual MAC technique applied. When the EDs are required to send a data frame, they immediately transmit the frame without any backoff and ignore the channel condition.

Case 2 serves as both a reference and a selective adaptation of CSMA/CA with a fixed DIFS. Before an ED attempts to transmit, a free DIFS is required; however, in this case, DIFS is replaced by two CAD procedures. In a related study, researchers

observed instances of false idle detection caused by the CAD process and recommended using nine CAD procedures to minimize such occurrences [46]. Their work focused on transmitting long packets in star networks, where retransmission of these lengthy packets incurs higher costs, resulting in lower collision tolerance. In contrast, this study aims to adapt CA techniques for mesh networks, emphasizing the efficient use of idle medium time over the complete prevention of collisions, and therefore allowing for a small tolerance for false idle detection.

However, CSMA/CA with a fixed DIFS is not well suited for mesh network scenarios. After an ED completes its transmission, all NEs begin sensing the same medium using the same number of CAD procedures. As a result, all extenders may perceive the medium as idle and initiate their transmissions simultaneously. To address this, an ALOHA-based or CSMA-based MAC protocol in a mesh network should incorporate an initial random backoff period.

Case 3 incorporates randomness into S-ALOHA, based on a concept from a previous study [43]. In this method, EDs are permitted to transmit only at the start of the next time slot. The duration of each slot ($T_{slot}$) must exceed the maximum Time on Air ($ToA$) for LoRa packets, which means that transmissions can only occur at the beginning of a $N_r$ generated prior to each transmission. While this approach helps mitigate collision issues, it does not effectively utilize the idle medium. If a large $N_r$ is generated, it can result in significant wastage of idle medium, leading to inefficiencies in network resource utilization.

In case 4, randomness is introduced into the CSMA protocol. Instead of utilizing two fixed CAD procedures as in DIFS, we employ 2 $N_r$ CAD procedures. The use of CAD in CSMA/CA draws from previous studies [46]-[49]. This approach enhances the efficient use of idle medium, contributing to a reduction in collision occurrences.

However, both Cases 3 and 4 depend on generating different $N_r$ values for all nearby

NEs. As the number of NEs within range increases, the likelihood of generating identical $N_r$ values also rises, leading to potential collisions. This inherent limitation can be addressed and further improved in Cases 5 and 6.

In case 5, the random number $N_r$ is replaced with uniquely assigned slot numbers $N_s$. This concept of using unique slot numbers is adapted from a previous study [44]. NE can be assigned an $N_s$ starting from 0 when it joins the network, which eliminates the excessive waiting times associated with generating a large $N_r$ in Case 3.

With this approach, EDs are able to transmit after $N_s$ slots, meaning that no collisions between NEs are anticipated when only one transmission is initiated. However, this method does not address the potential collisions that may occur if two EDs attempt to transmit simultaneously.

In case 6, the two fixed CAD procedures are replaced by $N_s$ CAD procedures. As a NE continuously monitors the medium, this design becomes more resilient to collisions that may occur when multiple EDs attempt to send packets simultaneously. This setup represents the final form of the proposed MAC protocol and is anticipated to outperform the previous iterations.

Cases 1 and 2 are exclusively applicable to star networks and are not feasible for mesh networks, as they cannot effectively avoid collisions among NEs.

In contrast, Cases 2 to 6 are designed for mesh networks, allowing for collision avoidance among NEs. Cases 3 and 4 utilize random backoff methods, while Cases 5 and 6 implement systematic backoff, necessitating the careful assignment of non-repeating $N_s$. As a result, Cases 3 and 4 are advantageous in scenarios that require quick setup. On the other hand, Cases 5 and 6 are anticipated to perform better overall; however, they demand significantly longer setup, testing, and correction times.

In the next section, we will discuss the implementation of the designed MAC protocols in hardware and the experiments conducted to evaluate their performance in

laboratory conditions.

## 3.3. Experiment setup

### 3.3.1. Hardware development of LoRa devices

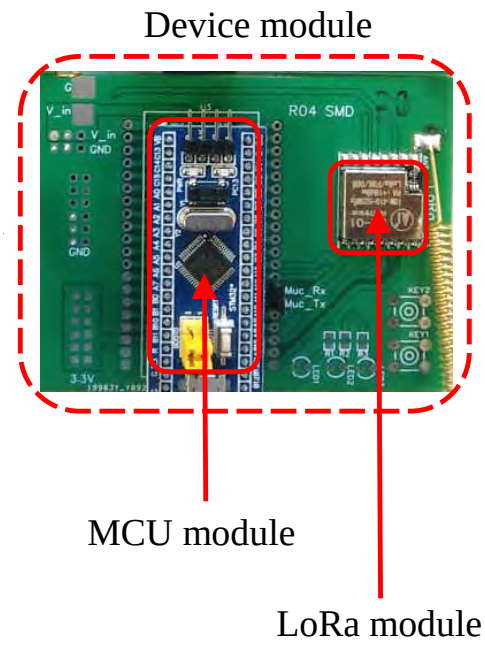


Figure 3.5 Photograph of LoRa module and MCU module in device module used as end point and gateway.

In this section, the experimental setup is described. The main goal of this study is to investigate and improve the medium access strategy based on the existing LoRa PHY specification. Therefore, a commercial LoRa chipset was selected to conduct experiments. Various brands of LoRa chipsets are available on the market, such as Texas Instruments, Microchip, and Semtech. Semtech's SX1278 was ultimately selected as the LoRa module because Semtech is the originator of the LoRa PHY. In addition, Semtech's LoRa transceiver provides the CAD function, which has been reported to be capable of detecting the payload using CAD. [46].

The mainstream microcontroller unit (MCU) STM32F103 was chosen as the MCU module to control the LoRa module. The same LoRa and MCU modules were used in the gateway to initiate transmissions and receive responses from EDs. In real applications, low-power MCU series are more desirable, as battery life is another major concern for IoT products. In addition, the transceiver in the gateway should be powerful enough to support concurrent reception on multiple channels with different SFs and carrier frequencies. For instance, the SX13XX series products from Semtech are more suitable for gateway development. However, concurrent listening and battery life extension are not the focus of this research.

Finally, a printed circuit board (PCB) was designed to integrate the selected MCU and LoRa modules to form the device modules (EDs and gateway) shown in Figure 3.5. The PHY and CAD requirements could be met with a relatively small amount of hardware setup. Moreover, since the LoRa module handles only the PHY layer, the MCU firmware can freely implement different medium access methods.

| | |
|---|---|
| **Spread factor (*SF*)** | 7 |
| **Bandwidth (*BW*)** | 500 kHz |
| **Coding rate (*CR*)** | 4 |
| **Carrier frequency** | 433 MHz |
| **Preamble length** | 6 byte |
| **Payload length** | 30 byte |
| **Explicit header** | On |
| **payload CRC** | On |
| **Theoretical payload bit rate** | 13671 bps |

Table 3.5 LoRa module configuration

After the completion of hardware implementation, the LoRa PHY configuration is fulfilled. The parametric selection is listed in Table 3.5. The *SF* was set to be the minimum, and *BW* was set to be maximum, so that theoretical $R_b$ could be maximized

by sacrificing the total link budget. *CR* was also maximized to increase the robustness of data frames by reducing the theoretical $R_b$. Combining all effects of significant factors, 13671 bps should be reached in theory. The test data frame was configured to be 30 bytes payload, 6 bytes of programmable preamble length, explicit header turned on, and payload CRC added. The actual *ToA* was around 50 ms for a complete frame.

### 3.3.2. Medium Occupancy Test

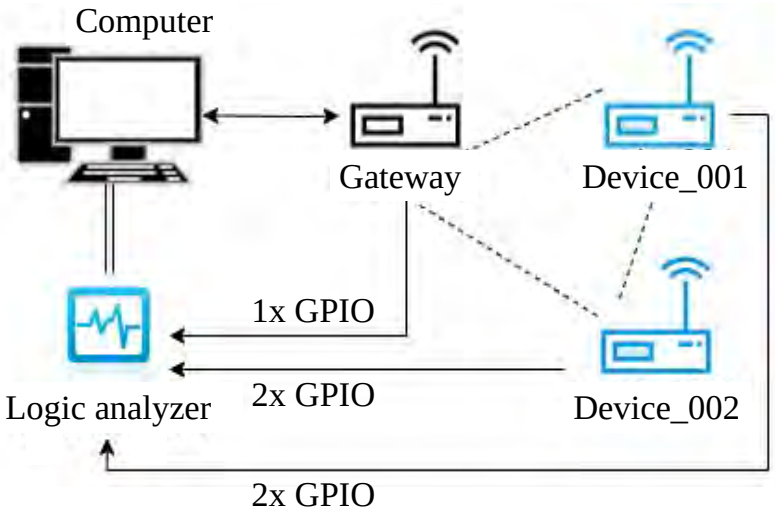


Figure 3.6 Experiment setup for medium occupancy test.

The medium occupancy test is designed to clarify how collisions occur and why one MAC performs better than another. In addition, collision patterns and medium occupancy patterns can indicate how efficiently the medium is utilized. The test setup is shown in Figure 3.6. The general-purpose input/outputs (GPIOs) of the EDs and the gateway are connected to a logic analyzer. When the gateway and EDs are transmitting a data frame, one of their GPIOs is driven high for the duration of the transmission.

An additional GPIO on each ED is also connected to the logic analyzer and toggles its state when CAD procedures are being conducted. When the required number of free CADs is met, this second GPIO on the ED is reset. By plotting the logic states of the

five GPIOs, the presence of collisions can be observed from the transmission GPIOs of the EDs. Consequently, the efficiency of medium occupancy can be evaluated.

### 3.3.3. Collision Test

| | |
|---|---|
| **System size** | 30 NEs |
| **Transmission Interval ($T_{tx}$)** | 10/6/3 s |
| **Random number ($N_r$)** | [1–150] |
| **Assigned number ($N_s$)** | 1 for NE1, 2 for N2<br>… 30 for NE30 |
| **Time slot duration ($T_{slot}$)** | 100 ms |
| **Message length** | 30 bytes |
| **Actual Time on Air (*ToA*)** | ~50 ms |

Table 3.6 parameters of collision tests setup

The collision test is designed to measure the PDR, with parameters listed in Table 3.6. This test setup includes 1 ED and 30 NEs within the ED's coverage area, creating a more contentious environment than typical real-world applications. Generally, one NE per area suffices for extending a mesh network. In cases where environmental changes disrupt the connection between an NE and the ED, two to four additional NEs are added as buffers. The large number of NEs in this test aims to amplify the differences observed among the six cases.

During the collision test, the ED periodically broadcasts a 30-byte data frame to the NEs at transmission intervals ($T_{tx}$) of 500, 400, 300, and 200 ms. This setup simulates heavy traffic conditions with a limited number of NEs. All NEs respond to the fixed 30-byte data frame, which includes their device ID. The random number $N_r$ is an integer ranging from 1 to 150, while the unique numbers $N_s$ are assigned as 1 for NE1 and 2 for NE2. Given that the *ToA* for the 30-byte data frame is approximately 50 ms, $T_{slot}$ is set to 100 ms for cases without CAD.

The calculations for the PDR and channel traffic (G: packets per second) are

represented by Equations (2.1) and (2.2), respectively.

$$\text{PDR} = P_{received} / P_{sent} \quad (2.1)$$

$$G = P_{sent} / T_{test} \quad (2.2)$$

The PDR is calculated using the number of received packets divided by the number of sent packets. The channel traffic is calculated by dividing the total sent packets by the test duration [43].

## 3.4. Experiment Result

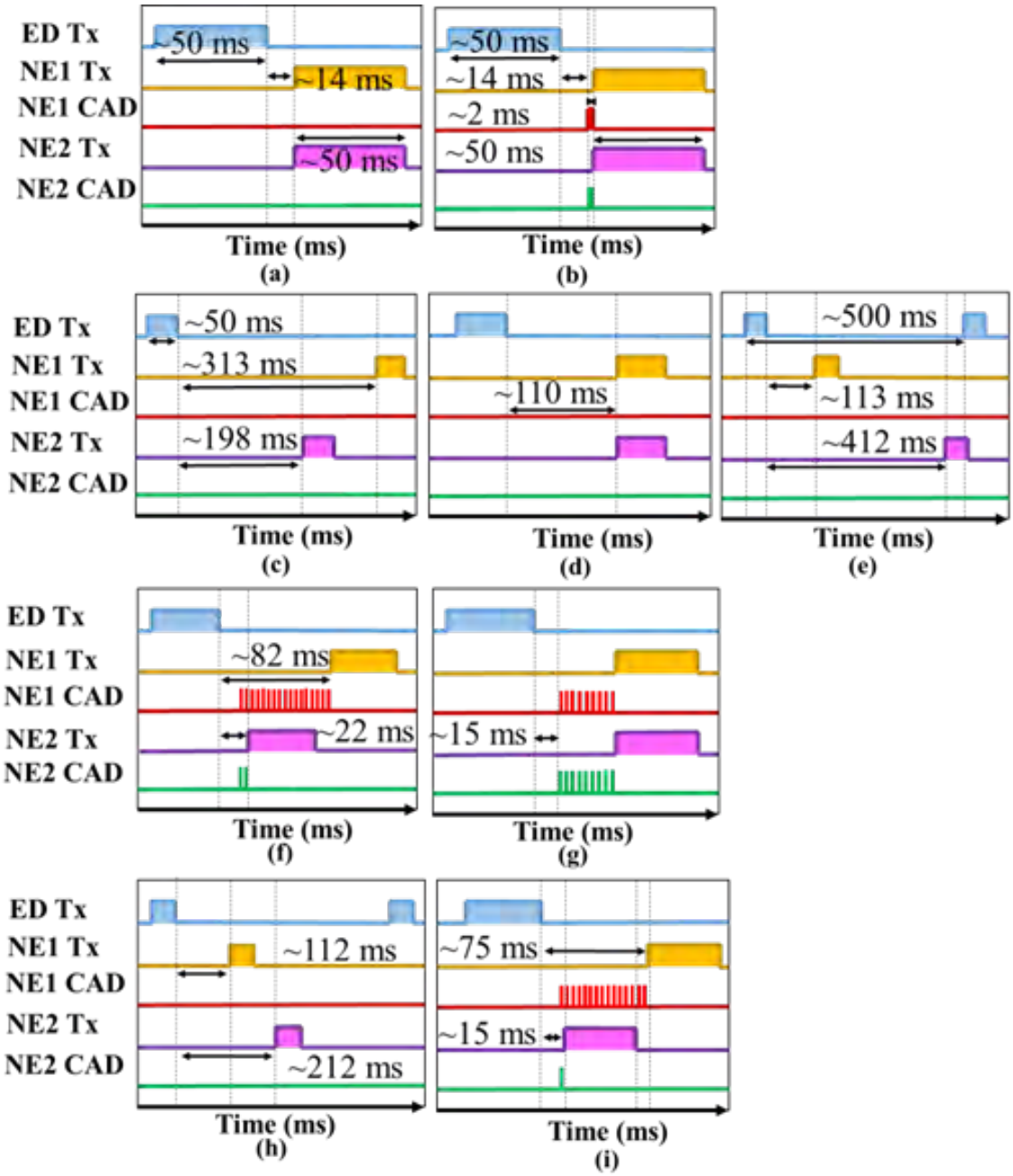


Figure 3.7 Typical results of medium occupancy test.

In Figure 3.7, the GPIO states of the ED and NEs are plotted in the following sequence: ED Tx, NE1 Tx, NE1 CAD, NE2 Tx, and NE2 CAD. This sequence refers to channels 1–5 in the logic analyzer.

### 3.4.1. No MAC

As shown in Figure 3.7(a), channel 1 is activated, indicating that the ED is initiating a transmission. Subsequently, channels 2 and 4 are driven high, indicating that NE1 and NE2 are attempting to send packets immediately after the ED completes its transmission. However, since channels 2 and 4 overlap during this period, a collision occurs. Without a random delay or some form of coordinated delay, collision-free transmission becomes impossible.

This collision pattern consistently appears due to the repetitive nature of the MAC logic. As a result, the PDR remains close to zero, despite the unique collision tolerance mechanisms of LoRa technology and the robustness of the LoRa PHY. In addition to the collisions and the time-on-air (*ToA*) of the data frame, a reception delay of approximately 14 ms is also observed, primarily due to communication between the LoRa and MCU modules.

### 3.4.2. CSMA/CA with fixed DIFS

As shown in Figure 3.7(b), the GPIO states for channels 3 and 5 toggle from low to high and then back to low after the ED's transmission. This indicates that both NE1 and NE2 have completed two CAD procedures. Since both NEs initiate the CAD procedure simultaneously, they both perceive the medium as free for transmission. Consequently, a collision remains inevitable, even with the implementation of the LBT strategy.

The results from Cases 1 and 2 further highlight the necessity of introducing either a random or coordinated delay to effectively prevent collisions between NEs.

### 3.4.3. S-ALOHA with random slots

S-ALOHA with the random number $N_r$ is utilized in the transmission process. As illustrated in Figure 3.7(c), collision-free transmission is achieved when NE1 selects an $N_r$ value of 3 and NE2 chooses an $N_r$ value of 2. The random generation of different

numbers allows the two data frames to occupy distinct time slots. NE1 begins its transmission after waiting for approximately 200 ms, while NE2 waits for about 300 ms, given that the time slot duration is set to 100 ms. However, when the same $N_r$ value is generated, a collision occurs, as shown in Figure 3.7(d). Although the probability of selecting the same number decreases with an increased range of $N_r$, opting for a larger number can lead to prolonged waiting times and may result in collisions during subsequent ED transmissions, as depicted in Figure 3.7(e). Consequently, S-ALOHA may not be sufficiently effective when data frames are transmitted frequently.

### 3.4.4. CSMA/CA with random DIFS

CSMA/CA with the random number $N_r$ is evaluated. In case 2, simply applying CAD proves ineffective when all NEs are activated simultaneously. To address this, randomness is incorporated into case 2. As shown in Figure 3.7(f), different $N_r$ values are generated, necessitating varying numbers of idle CAD procedures for NE1 and NE2. NE2 initiates its transmission after completing four CAD procedures, taking only ~22 ms. In contrast, NE1 requires additional CAD procedures due to the random selection of a larger $N_r$. When NE2 begins transmission, the CAD procedures identify the busy medium, preventing NE1 from transmitting to avoid a collision. After NE2 concludes its transmission, NE1 starts after completing six more CAD procedures.

Case 4 demonstrates a more efficient use of the idle medium compared to case 3. Even with larger Nr values assigned to NE1 and NE2, case 4 experiences lower latency. This improvement is attributed to minimizing the DIFS in CSMA/CA to 2 ms, rather than the minimum of 50 ms, which corresponds to the longest data frame's *ToA*. Additionally, estimating the maximum *ToA* can be challenging in real-world applications where the payload length varies. Overestimating the maximum *ToA* can further diminish the efficiency of idle medium utilization. Conversely, underestimating the longest data frame *ToA* cannot eliminate collisions, even with different $N_r$ values.

This inaccurate estimation undermines the feasibility and effectiveness of CA in S-ALOHA.

### 3.4.5. S-ALOHA with assigned slots

In this scenario, the assigned number $N_s$ is utilized to address the issue of generating identical $N_r$ values. $N_s$ values of 1 and 2 are designated for NE1 and NE2, respectively. As illustrated in Figure 3.7(h), NE1 and NE2 wait around 100 ms and 200 ms before transmitting to prevent collisions. Ideally, this condition should be consistently repeated; no random $N_r$ should be employed, which would lead to a theoretical PDR of 100%. However, since the data length can vary, the *ToA* may not always be less than the $T_{slot}$.

### 3.4.6. CSMA/CA with assigned DIFS

This case aims to integrate the benefits of Cases 1 through 5. Cases 1 and 2 highlight the need for a non-persistent strategy to resolve collisions among NEs. Case 3 illustrates how random backoff can help prevent collisions. Case 4 demonstrates the effectiveness of CSMA/CA using a random number of CAD procedures, while Case 5 shows that an assigned backoff can further minimize collision risks. The proposed method in this case involves applying non-persistent CSMA/CA with a designated number of CAD procedures.

As shown in Figure 3.7(i), NE1 and NE2 complete four and two idle CAD procedures, respectively, before transmission. The distinction between Cases 5 and 6 mirrors that between Cases 3 and 4. MAC protocols employing CAD are more efficient in utilizing idle medium time and offer greater flexibility than those without CAD, making them suitable for networks with variable data lengths.

### 3.4.7. Collision Test Result

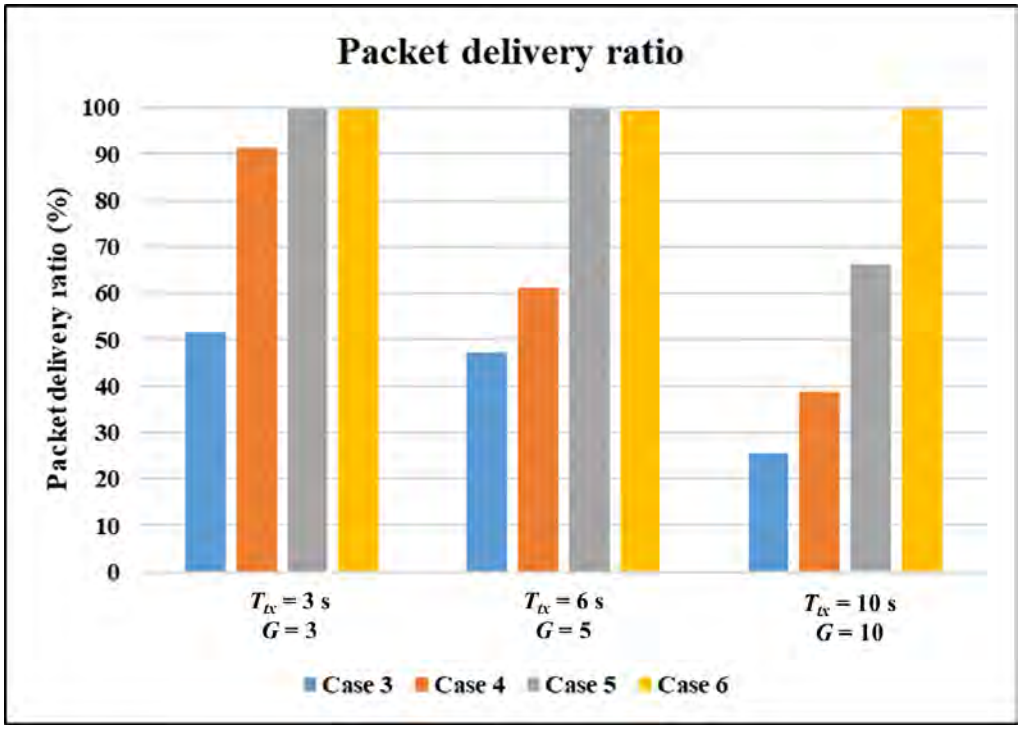


Figure 3.8 PDRs of proposed MAC protocols under different transmitting intervals ($T_{tx}$).

Figure 3.8 presents the PDRs in percentage for four MAC protocols within a system comprising 30 NEs. Cases 1 and 2 are omitted, as all data packets collide following ED transmission.

In case 3, the PDR hovers around 50% when the $T_{tx}$ is 10 seconds but drops to about 25% when $T_{tx}$ is reduced to 3 seconds. Conversely, case 4 achieves a PDR of approximately 90% at $T_{tx}$ equals to 10 s, falling to 40% at $T_{tx}$ equals to 3 s. The less-than-unity PDRs in both cases indicate that collisions occur during the tests, as illustrated in Figure 3.7(d) and 3.7(g), where packet collisions arise from multiple NEs generating the same random number.

Case 4 outperforms case 3 by better utilizing the available medium. The reduction in $T_{tx}$ results in a higher traffic load G within the channel, making a MAC protocol that efficiently uses idle medium more effective. Cases 5 and 6 exhibit nearly 100% PDR when $T_{tx}$ is 10 and 6 seconds, respectively. However, as $T_{tx}$ decreases further to 3

seconds, case 6 maintains a PDR of around 100%, whereas case 5 sees a significant drop to approximately 70%.

Both Cases 5 and 6 avoid the issue of identical Nr values, which was problematic in Cases 3 and 4. Consequently, they achieve approximately 100% PDR when Ttx exceeds 6 seconds. However, when Ttx is further reduced to 3 seconds, equivalent to 30 time slots, the guard time between the last and the next ED transmission becomes insufficient. If the transmission from NE30 overlaps with the subsequent ED transmission, not all 30 NEs will be transmitted in the following round, which is a disadvantage for Case 5.

In practical scenarios, multiple EDs may initiate transmissions within a short period, and an effective MAC protocol should be able to accommodate this. Additionally, while fixed packet lengths benefit Cases 3 and 5, this assumption often does not hold in real applications. In contrast, Cases 4 and 6 employ CSMA/CA with CAD to manage collisions among multiple EDs, handle varying packet lengths, and utilize idle channel time more effectively.

The low PDRs in the other cases primarily stem from highly contentious test conditions rather than limitations of the protocols themselves. Overall, the MAC protocols evaluated outperform P-ALOHA in the LoRaWAN context. Furthermore, deploying a dense concentration of NEs in a single area is typically discouraged; in practice, one NE is sufficient, with two to three redundant NEs in proximity to ensure network resilience if some fail. The use of an unrealistically high number of NEs in this study was intended to highlight the differences between cases 2 and 6.

This section analyzes the typical medium occupancy patterns and PDRs for four MAC protocols in mesh networks. The progression from case 3 to case 6 illustrates how each feature in the MAC protocols contributes to collision avoidance. Ultimately, case 6 exhibits optimal performance, achieving approximately 100% PDR when $T_{tx}$ is 3

seconds, and the G is 10 packets per second. Consequently, 2 $N_s$ CAD procedures are executed to implement CSMA/CA before transmitting the ED's packet. Thus, the proposed MAC protocol effectively utilizes idle mediums while accommodating packets of varying lengths.

## 3.5. Section Summary

LoRa networks offer significant advantages, such as wide coverage and high resistance to noise, but they currently lack a public mesh protocol. As a result, other wireless mesh solutions can surpass the coverage offered by LoRa networks. Although researchers have explored mesh structures and collision handling for LoRa, studies specifically focused on collision handling in mesh networks are still limited. This gap presents an opportunity for further research and development to enhance the capabilities of LoRa networks in mesh configurations.

In this study, we proposed protocol-independent, mesh-specialized CSMA/CA methods for LoRa mesh networks. Six MAC methods were tested. Case 6 demonstrated strong performance across all tested conditions and is recommended as the most effective MAC method presented in this chapter. However, each MAC method has its own strengths in specific scenarios.

Case 3, based on slotted ALOHA with a random backoff, is the simplest method and requires the least effort to implement. If the selected LoRa module can quickly determine channel occupancy, Case 4 would be a better choice for improving PDR. Both case 3 and case 4 do not have comparable performance with case 5 and case 6, they are still necessary before unique $N_s$ are assigned to each end device. The unique $N_s$ assigning process is usually possible after the end devices joining the gateway's network. Broadcast network joining invitations could be responded by multiple end devices at the same time through implementing MAC in case 3 or case 4.

After joining the network, both Case 5 and Case 6 become applicable. Although nearly 100% PDR can be achieved by both methods under most conditions, only Case 6 is able to maintain almost 100% PDR under extreme conditions with insufficient response time. This is because the method in Case 6, which uses CAD, achieves more efficient utilization of idle medium time. Furthermore, methods that employ CAD are more flexible than those without CAD, as they remain applicable in systems with varying payload lengths. Therefore, Case 6 is recommended over the other MAC methods when all prerequisites for Case 6 are satisfied.

Moreover, once the network is formed, it is not necessary to continuously enable periodic gateway beacons. Constant beacons are best suited for applications that require regular synchronization of end device status, such as air-quality monitoring sensor networks. However, for end devices designed to send notifications only when their status changes, constant beacons are unnecessary. For instance, in a water or gas leakage monitoring system, frequent data synchronization is not required; instead, end devices should transmit alerts to the gateway only when an emergency event occurs.

Heartbeat beacons should be sent a few times per hour to confirm that there are no malfunctions in the end devices. Additionally, networks with actuators should primarily rely on heartbeat beacons and remain mostly idle while waiting for downlink commands from servers or users, as in lighting control systems. Constant beacons can delay real-time user commands, leading to noticeable lag.

In the scenarios mentioned above, both Case 4 and Case 6, which use CAD-based CSMA/CA, are recommended during non-beaconing periods. Conversely, Cases 3 and 5 are not advisable due to their excessive waiting times, which ignore actual channel usage and the possible absence of other active end devices. This unnecessary delay can negatively impact response times, severely affecting user experience and overall system performance, particularly in real-time applications.

# 4. WATER FLOOD SENSOR DEPLOYMENT OF THE PROPOSED NETWORK IN A COMMERCIAL BUILDING

## 4.1. Introduction

In Chapter 2, we examined how SAW filters can enhance the stability of end devices at the circuit level. Chapter 3 focused on how MAC protocols can optimize network performance in terms of Packet Delivery Ratio (PDR) at the system level. In this chapter, we integrate insights from these previous discussions and broaden our study to encompass not only academic perspectives but also practical applications for commercial use.

At the circuit-stability level, in-house fabricated filters lack the ability to be mass-produced with consistent quality control. As a result, we utilize equivalent inductors and capacitors implemented with discrete components, even though they may require more space on the PCB. At the system-stability level, we have chosen to implement the Case 4 MAC protocol for the application. The rationale for selecting Case 4 to establish a mesh network, instead of Cases 5 or 6, will be addressed in a later section.

A long-term system deployment project has been launched in an operational commercial building in partnership with the property management company. This initiative includes 205 end devices and a single gateway covering 23 continuous floors. Water-flood detection sensors are installed on these floors to notify the property management team, enabling a swift response to prevent significant losses and avoid flooding that could damage expensive equipment such as elevators and escalators.

This deployment serves two main objectives. First, for commercial purposes, it aims to establish a centralized IoT water-flood detection system throughout the building.

Second, for research purposes, it is designed to test the mesh network in a real-world environment characterized by noise and uncertainty, allowing us to evaluate the reliability of the proposed mesh network.

## 4.2. Hardware development

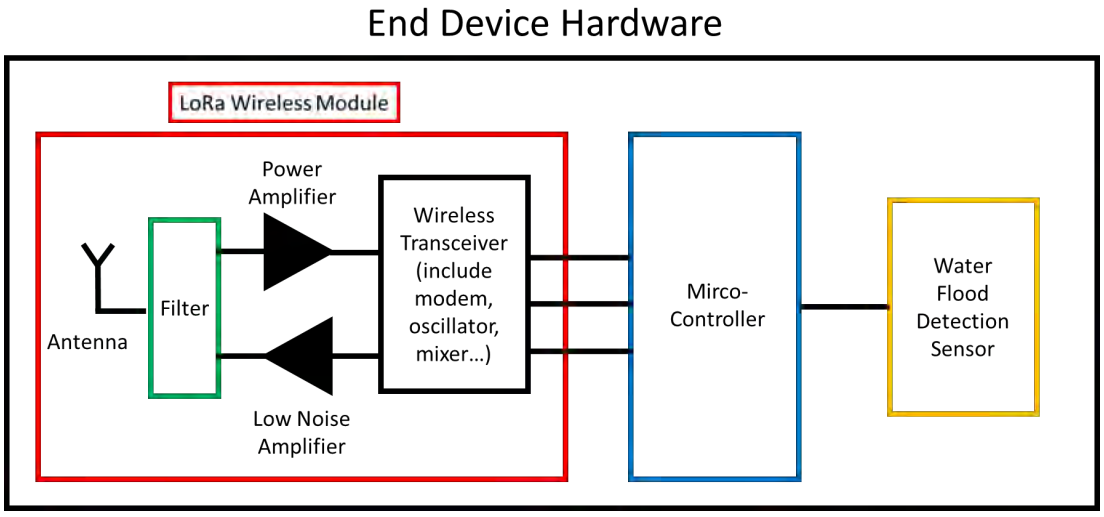


(a)

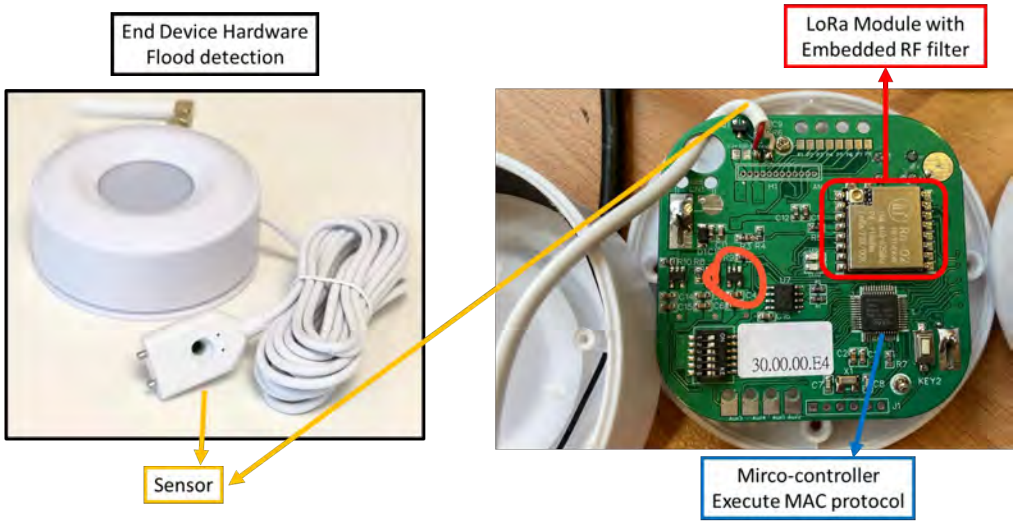


(b)

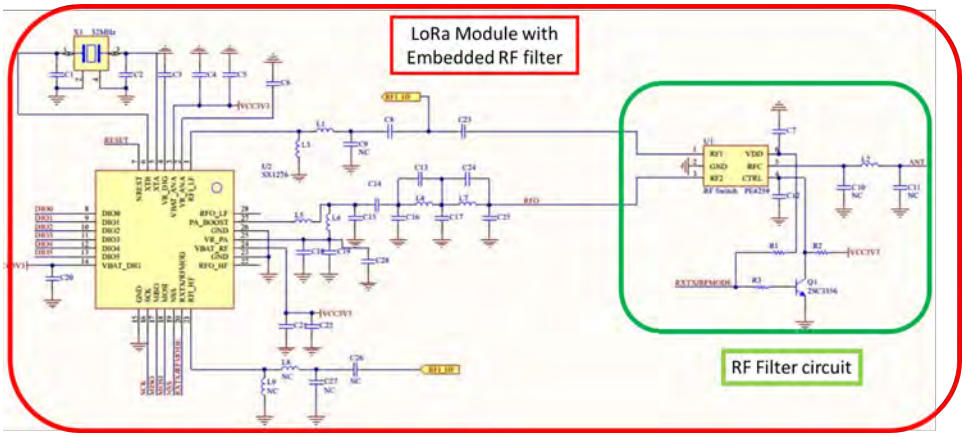


(c)

Figure 4.1 Tailored Flood sensor for deployment (a) block diagram (b) actual hardware appearance (c) RF filter schematic

In Chapter 1, we presented a general block diagram of an IoT device. This diagram has now been modified to incorporate a flood detection sensor, tailoring it into a specific end device (ED) for flood detection applications. The updated block diagram is illustrated in Figure 4.1(a). The water-flood ED has been designed and fabricated according to this block diagram, as shown in Figure 4.1(b). A customized PCB has been developed to interconnect all the essential electronic components required for its operation.

The PCB includes a LoRa module, which features an embedded RF filter within its metallic enclosure, as depicted in Figure 4.1(c). This RF filter is designed to reject environmental noise outside the desired frequency band, facilitating smoother and more reliable packet transmission. Although this RF filter is not a SAW filter, it serves a similar purpose, as discussed in Chapter 2.

The PCB also contains an MCU, which executes the MAC protocol, the primary focus of Chapter 3. This MCU is essential for managing communications and ensuring the efficient operation of the flood detection application.

Figure 4.2 Protective cover for the water leakage sensor

Moreover, the PCB connects the flood sensor via soldering pads, which link directly to the MCU. The sensor comprises two metallic probe heads connected to two

separate wires. Under low-voltage conditions, such as 3.3 V, it can be assumed that the resistance between the two metallic probes is effectively infinite. However, when water bridges the gap between the probes, this resistance becomes finite, typically on the order of a few megaohms. This change in resistance enables the detection of water presence, signaling an alert to the MCU.

To further enhance reliability, a protective plastic cover is installed in front of the flood sensors, and the sensor probes are positioned 3 mm above the ground to minimize the risk of false triggers from daily cleaning routines, as shown in Figure 4.2.

Each ED consumes around 30 μA at 4.5 V (using three AAA 1.5 V batteries with a capacity of approximately 800 mAh) in sleep mode. In receive (Rx) mode, it consumes about 20 mA, and in transmit (Tx) mode, it draws 150 mA. The EDs remain in sleep mode for most of the time, waking up in Tx mode once per hour. After each Tx operation, they switch to Rx mode for a few seconds to receive an acknowledgment before returning to sleep mode. Given this operational pattern, the expected battery life of each ED is projected to exceed two years.

## 4.3. Deployment plan

### 4.3.1. Installation plan

The backbone of the mesh network consists of 46 NEs and one gateway, which connect 159 EDs—battery-powered water-flood sensors installed inside toilets. The single mesh network spans 23 continuous floors, from L9 to L35 (excluding L14, L24, and L34). In total, 205 devices, including NEs and EDs, are installed.

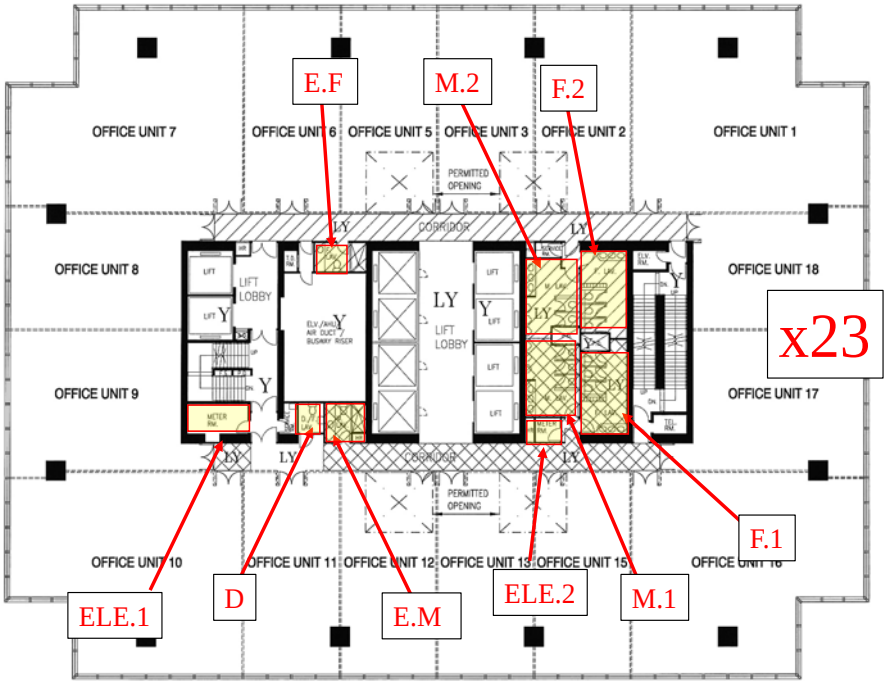


Figure 4.3 Deployment site typical floor plan and installation plan

Figure 4.3 shows the typical floor plan of L9–L35. Each typical floor includes two NEs and seven water flood sensors. Two NEs are installed in electric room 1 (ELE.1) and electric room 2 (ELE.2). The seven water flood sensors are installed at the male executive toilet (M.E), female executive toilet (F.E), male toilet 2 (M.2), male toilet 1 (M.1), disable toilet (D), female toilet 2 (F.2), and female toilet 1 (F.1).

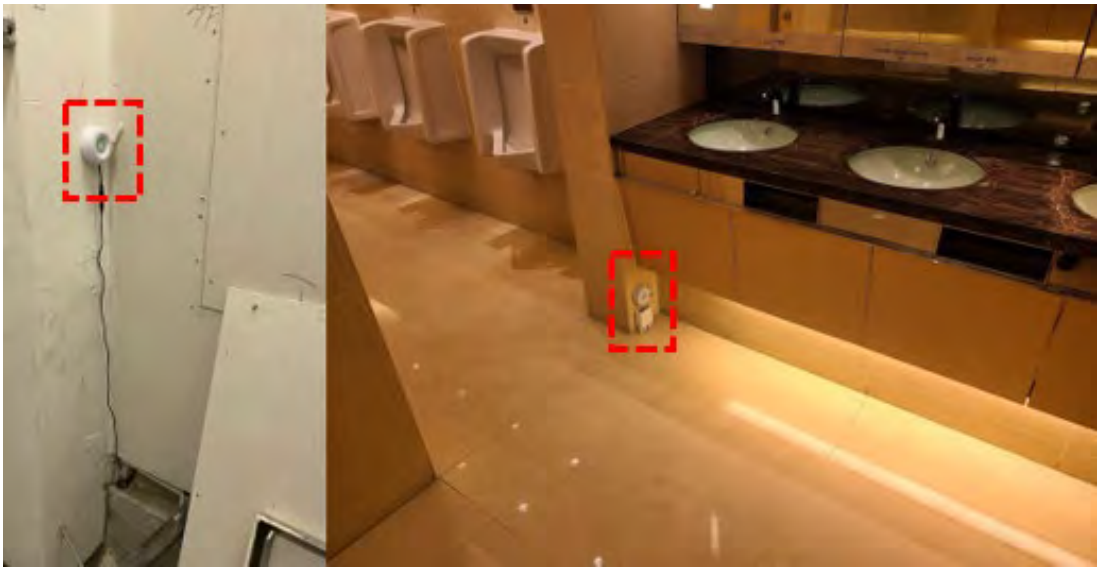

Figure 4.4 Actual installation of NE in electric room (left) and water flood sensor with built-in battery as ED in male toilet (right).

Figure 4.4 shows that water-flood sensors are installed in the male toilets, while NEs are located in the electrical rooms on each floor, facilitating vertical connections within the mesh network. An elevator shaft is located in the middle of the building, which significantly reduces signal strength for transmissions across the same floor. To ensure coverage, an additional NE is installed on each floor. On L32, the NE for ELE.1 is replaced by the gateway.

NEs must remain active continuously to forward messages in the mesh network, whereas water-flood sensors can enter deep sleep mode to conserve power. Therefore, NEs are installed in electrical rooms where power sockets are available, while the battery-operated water-flood sensors, with a lifespan exceeding two years, can be installed directly in toilets where no power sockets are present..

### 4.3.2. System Setup

The data collection period for the experiment spans from July 2023 to December 2023, covering six months of data. The data from the water-flood sensors are recorded and evaluated. Water-flood detection is one of the applications of the proposed LoRa mesh network. Other sensors can also be used, such as electric valves and indoor air-quality sensors. However, these sensors or actuators tend to be more expensive and are therefore usually limited in quantity. In contrast, water-flood sensors are low-cost, allowing for larger-scale deployment. For this reason, the water-flood detection application is chosen to demonstrate the capability of the proposed network. Additionally, the focus of this deployment is on network performance rather than on flood-sensing technology itself.

Regarding latency, each hop requires approximately 0.2 seconds. This duration accounts not only for the time-on-air (ToA) of the packet but also for the time spent on MCU program logic execution and CAD checking procedures.

In the worst-case scenario, a maximum of 11 hops is needed for an ED on L21 to reach the gateway on L32. It is assumed that each hop penetrates only one floor; however, in practice, packets can often penetrate two to three floors directly. Therefore, the maximum latency is approximately 4.5 seconds, while the nominal latency is less than 2 seconds, depending on the number of hops required to reach the gateway.

Each ED sends a 70-byte packet once per hour, which is received and retransmitted by the NEs to the gateway. The gateway then forwards the message to the cloud server and stores it in a database. With 159 water-flood sensors and 46 NEs installed, a total of 205 individual packets are sent per hour. Each of these packets is retransmitted once by the 46 NEs, resulting in 9,430 packets traveling through the mesh network each hour. Using Equation (3.2), we can calculate G=2.62 for this application scenario.

Each packet includes a sequential incremental packet number that starts when the

device is powered on. The total number of packets can be determined by subtracting the packet number recorded at the end of the day from the initial packet number. By comparing these sequential values in the database, any missing packets between the received packets can be identified. This allows the Packet Delivery Ratio (PDR) to be calculated using Equation (3.1).

A monitoring system was also developed, and its web platform is shown in Figure 4.5(a). Each device's condition, including online/offline status, and battery level is in Figure 4.5 (b). If the water flood is detected, the status of the sensor's status will change as shown in Figure 4.5 (b). And the monitoring system will send an alert directly by mobile messages to related parties or users.


(a)

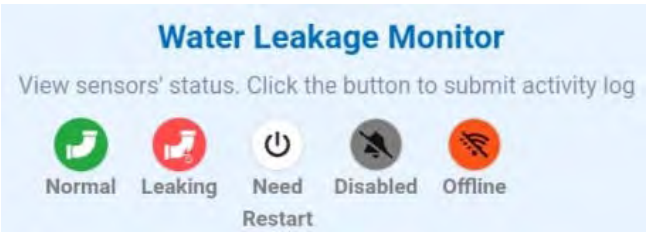


(b)

Figure 4.5 Monitoring system: (a) Selected floors on each sensor's status and its battery level in platform and (b) each sensor's logo on its status.

### 4.3.3. Limitation

In this implementation, Case 4 is utilized instead of Cases 5 and 6 due to constraints set by the property owner. Cases 5 and 6 require assigning unique identifiers (Ns) to each device, including both NEs and EDs, ensuring that Ns do not repeat within the coverage area of any device.

Currently, these numbers are assigned manually by hardcoding. One straightforward approach is to assign each NE a unique N from 1 to 46, which is clearly an inefficient use of channel resources, as most NEs can directly communicate with only 4–6 neighboring NE. We could carefully test and assign $N_s$ of 1-6 to each NE. However, this process demands significant time for setup and verification. Given that most EDs are installed in tenant areas with limited installation periods provided by property management, the likelihood of errors, such as assigning the same Ns to two devices within range, increases. Such mistakes can lead to guaranteed collisions. Considering the complexity of setting up Case 6, especially with over 200 devices, only Case 4 was implemented. Due to the difficulties in setup, time costs, and potential for errors, Case 4, which uses $N_r$, is selected for this application. As shown in Figure 3.8, Case 4 ensures a PDR greater than 90% at G=3. Therefore, with G=2.62, we can expect a PDR exceeding 90% in general.

## 4.4. Deployment result

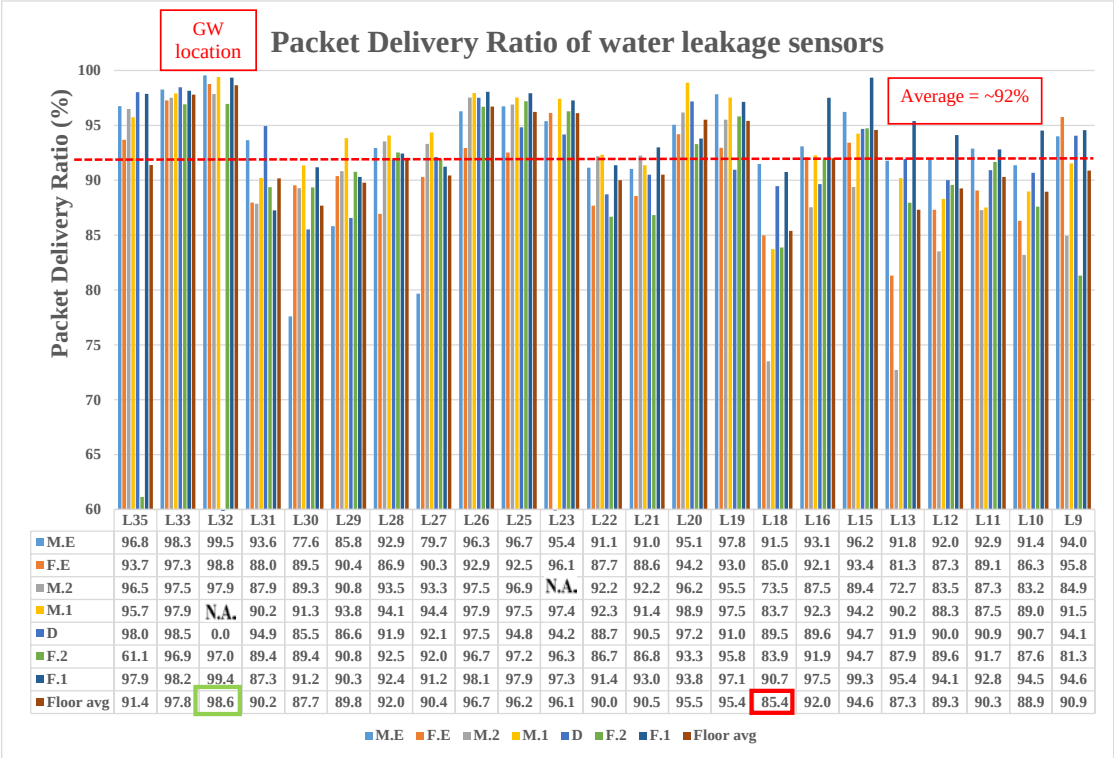


| | L35 | L33 | L32 | L31 | L30 | L29 | L28 | L27 | L26 | L25 | L23 | L22 | L21 | L20 | L19 | L18 | L16 | L15 | L13 | L12 | L11 | L10 | L9 |
|---|---|---|---|---|---|---|---|---|---|---|---|---|---|---|---|---|---|---|---|---|---|---|---|
| M.E | 96.8 | 98.3 | 99.5 | 93.6 | 77.6 | 85.8 | 92.9 | 79.7 | 96.3 | 96.7 | 95.4 | 91.1 | 91.0 | 95.1 | 97.8 | 91.5 | 93.1 | 96.2 | 91.8 | 92.0 | 92.9 | 91.4 | 94.0 |
| F.E | 93.7 | 97.3 | 98.8 | 88.0 | 89.5 | 90.4 | 86.9 | 90.3 | 92.9 | 92.5 | 96.1 | 87.7 | 88.6 | 94.2 | 93.0 | 85.0 | 92.1 | 93.4 | 81.3 | 87.3 | 89.1 | 86.3 | 95.8 |
| M.2 | 96.5 | 97.5 | 97.9 | 87.9 | 89.3 | 90.8 | 93.5 | 93.3 | 97.5 | 96.9 | N.A. | 92.2 | 92.2 | 96.2 | 95.5 | 73.5 | 87.5 | 89.4 | 72.7 | 83.5 | 87.3 | 83.2 | 84.9 |
| M.1 | 95.7 | 97.9 | N.A. | 90.2 | 91.3 | 93.8 | 94.1 | 94.4 | 97.9 | 97.5 | 97.4 | 92.3 | 91.4 | 98.9 | 97.5 | 83.7 | 92.3 | 94.2 | 90.2 | 88.3 | 87.5 | 89.0 | 91.5 |
| D | 98.0 | 98.5 | 0.0 | 94.9 | 85.5 | 86.6 | 91.9 | 92.1 | 97.5 | 94.8 | 94.2 | 88.7 | 90.5 | 97.2 | 91.0 | 89.5 | 89.6 | 94.7 | 91.9 | 90.0 | 90.9 | 90.7 | 94.1 |
| F.2 | 61.1 | 96.9 | 97.0 | 89.4 | 89.4 | 90.8 | 92.5 | 92.0 | 96.7 | 97.2 | 96.3 | 86.7 | 86.8 | 93.3 | 95.8 | 83.9 | 91.9 | 94.7 | 87.9 | 89.6 | 91.7 | 87.6 | 81.3 |
| F.1 | 97.9 | 98.2 | 99.4 | 87.3 | 91.2 | 90.3 | 92.4 | 91.2 | 98.1 | 97.9 | 97.3 | 91.4 | 93.0 | 93.8 | 97.1 | 90.7 | 97.5 | 99.3 | 95.4 | 94.1 | 92.8 | 94.5 | 94.6 |
| Floor avg | 91.4 | 97.8 | 98.6 | 90.2 | 87.7 | 89.8 | 92.0 | 90.4 | 96.7 | 96.2 | 96.1 | 90.0 | 90.5 | 95.5 | 95.4 | 85.4 | 92.0 | 94.6 | 87.3 | 89.3 | 90.3 | 88.9 | 90.9 |



Figure 4.6 PDR result of the installed EDs.

First, Figure 4.6 shows a Packet Delivery Ratio (PDR) ranging from 85.4% to 98.6% for each floor, with an average PDR of 92.0% for all EDs. This result is comparable to the experimental findings in Figure 6, which indicated around 90% PDR at G = 3. The observed PDR reflects the reliability of the proposed network, suggesting that laboratory tests can provide dependable performance predictions, even with a limited number of devices used for a short duration. Furthermore, the CMSA/CA using Nr has been demonstrated to be effective not only in laboratory settings but also in real-world environments, which are subject to various uncertainties, including human and environmental factors.

Second, we observe a relatively similar Packet Delivery Ratio (PDR) across all floors, which represents different layers of the mesh network. This indicates that the PDR does not significantly deteriorate with an increasing number of mesh layers. The

floor with the highest average PDR of 98.6% coincides with the location of the gateway (L32), while the floor with the lowest average PDR of 85.4% (L18) is situated further from the gateway. However, there is no clear trend of decreasing PDR in relation to the increased distance from the gateway. Thus, packet collision avoidance methods can be effectively applied, even in scenarios with a large number of mesh layers.

Third, the observed PDRs are below 100%. One effective method for increasing PDR is the implementation of Case 6 MAC. However, due to time constraints during the installation period, Case 6 was not utilized. Therefore, protocols and mechanisms that enable the remote setting of Ns, without the need for onsite configuration, are crucial for the practical application of Case 6 MAC. These protocols can leverage Case 4 MAC to assign Ns to EDs and NEs, facilitating smoother implementation and enhancing overall network performance.

In the context of laboratory experiments, the content of lost packets is not a concern, as all packets only contain dummy information. However, in the real-world application of water flood detection, every packet's information is critical. Therefore, EDs are designed to persistently send data until an acknowledgment from the gateway is received, with a limit on resends to ensure that flood events are reliably communicated to the building’s service operator. For flood event packets, the resend limit is set to infinite. While this brute-force approach may temporarily interfere with the transmission of other sensors and affect overall PDR and network stability, prioritizing critical alert messages is essential. This study does not aim to exploit such forceful tactics but rather to explore ways to optimize the use of limited channel resources for scalable mesh networks. Additionally, we can reduce the G of the channel to minimize the possibility of collisions.

Currently, the meshing mechanism for NEs involves repeating every message once. For instance, a water flood sensor located at L32 M.E, close to the gateway, does not

require meshing for its packets to reach the gateway. However, this results in 46 unnecessary transmissions each time, significantly congesting channel traffic. This scenario highlights the potential for reducing G to increase PDR and, more importantly, enhance network scalability, particularly for larger systems. To reduce unnecessary transmissions, NEs can be restricted to repeat messages only from certain EDs, necessitating a mechanism for assigning an ED list for specific NEs in the future. Despite these challenges, the system remains functional, demonstrating the effectiveness of the proposed MAC in managing collision risks, even with the current excessive packet transmission.

Finally, we observe some sudden drops in PDR at several installation sites, such as 61.1% at L35 F.1 and 72.7% at L13 M.2. However, these issues do not consistently repeat at different locations on the same floor or across different floors. This variability may be attributed to environmental or hardware issues, which are not inherent problems of the proposed MAC.

## 4.5. Discussion and Comparison

| Reference | This work | [23] | [24] | [35] | [36] |
|---|---|---|---|---|---|
| **Number of devices in Deployment** | 205 | Test 1: 5 devices<br>Test 2: 16 devices | 16 | 39 | 6 |
| **Location** | Commercial Building (23 floors) | City drainage system (typical / max 2 hops) | Campus (800 m × 600 m) | Campus (7 floors) | Campus (max. 2 hop) |
| **Packet Size (Byte)** | 70 | 26 (typical)<br>–51 (max) | 20 | 8 | 25–256 |
| **Test Scale (Time)** | ~ Half year | Field test 1:<br>23 days with 5 devices<br>Field test 2:<br>45 days with 16 devices | 200 packets for each sensor | N.A. | 50 packets (Multihop tests) |
| **SF Channel (Number of SF used at once)** | SF7 (1) | SF9 (1) | SF12 (1) (Campus scale test) | SF7–12 (6) | SF7, SF9 (6) |
| **Overall PDR** | 92 % | ~98 %<br>(~2 % error rate) | 88 % | ~90 % | 1 hop SF9 100 %<br>2 hops SF9 ~90 %<br>1 hop SF7 90 %<br>2 hops SF7 ~70 % |

Table 4.1 Comparison of mesh network performance with previous studies

Table 4.1 presents a comparison of our results with previous studies. Not many experiments have been conducted with a large number of devices and mesh hops; however, our experiments maintain a sufficiently high practical PDR. The proposed MAC protocol achieved a PDR of 92%, which is comparable to or even outperforms most of the previous research.

For instance, an 88.49% PDR was recorded in a trial involving a 19-device mesh network on a campus [24]. By contrast, our research achieved a slightly higher PDR with a substantially larger 200-device mesh network in a commercial building. Additionally, while their campus mesh network operates in a relatively open

environment, ours must navigate numerous signal-blocking structures inside a building. Despite a tenfold increase in system size and a more complex environment, we have obtained improved PDR. Moreover, our system has been operating stably for more than half a year amid uncontrollable and unpredictable events.

Another group of researchers proposed a spread-factor clustering approach to establish a stable LoRa mesh network [35]. Their network spanned two buildings across seven floors and comprised 36 devices, achieving approximately 90% PDR. Our study surpassed this PDR with a considerably larger system, although with a key difference. They utilized SFs 7–12, whereas we only used SF 7. The six SFs they employed can transmit simultaneously without mutual interference, meaning that in the best-case scenario, each SF channel accommodates only six devices with six test packets. In contrast, we only utilize SF 7, which is the one most affected by collisions, with a packet size of around 70 bytes [35]. Despite these challenging conditions, we managed to achieve a slightly higher PDR.

Although 100% PDR was achieved in a study [36], their system was limited to only six devices operating simultaneously with a maximum of two hops (or two mesh layers). When the mesh layers were increased to two, the PDR significantly declined to 90%, indicating that system performance deteriorates drastically with additional mesh layers. In contrast, our 200-device system is tested across 23 floors while maintaining a PDR of 92%. This demonstrates the robustness and scalability of our approach in a more complex environment.

The last related research pertains to a city drainage system, where wireless signals are blocked by concrete structures, similar to our mesh network inside a commercial building [23]. They achieved a relatively high PDR of 98%. However, in their experiment, only one hop was required for the EDs to reach the gateway. If it takes five hops to reach the gateway and each hop maintains a 98% PDR, the total PDR along this

path would be approximately 90% (0.98 to the power of 5). Moreover, their deployment involved a maximum of 16 devices launched over 45 days. In contrast, our deployment encompassed more than 200 devices in a single mesh network that lasted half a year, with the farthest ED requiring more than 10 hops. Despite these challenges, we have been able to maintain a PDR of 92%.

In summary, the proposed case 4 CSMA/CA MAC outperforms most of the similar research, in terms of PDR, device number, test coverage and test duration.

## 4.6. Section Summary

We established a large-scale mesh network spanning 23 floors with 205 devices and one gateway. Data collected over six months were analyzed, revealing that the large-scale onsite experiment results were comparable to the laboratory test results. Moreover, the overall PDR of 92% represents improvement over previous research involving considerably larger system scales.

The following aspects could be explored in future work. First, while the proposed MAC focused on collision avoidance in inevitable contentious conditions within the mesh network, there is potential to reduce the likelihood of such contentious situations occurring. To achieve this, the proposed MAC protocols could be further integrated with existing mesh protocols that feature multiple SF allocations and optimal pathfinding. This integration would not only enhance the efficiency of the network but also significantly improve the scalability of LoRa mesh networks. By addressing both collision avoidance and contention reduction, future developments can lead to more robust and adaptable network solutions.

Second, the proposed MAC protocols have yet to be tailored to be byte-field-specific. The structure of the byte field remains undefined, along with the methods by which EDs and NEs form and join mesh networks, maintain connections with gateways,

and the mechanisms for assigning nodes $N_s$. Defining the byte field could follow the specifications of LoRaWAN or other private protocols, ensuring that the proposed MAC is compatible with existing networks. This alignment would facilitate smoother integration and interoperability, allowing for better utilization of current infrastructure while enhancing the functionality of the LoRa mesh network.

# 5. DISCUSSION AND CONCLUSION

In this article, we examined various aspects of the stability of an IoT system. We began by exploring the physical phenomenon of how microwaves propagate from air into a PCB. During this process, environmental noise inevitably infiltrates the PCB and mixes with the signal. From a physical standpoint, one way to mitigate this interference is by rejecting noise outside the desired frequency band, which led us to discuss SAW filters. We designed, simulated, fabricated, measured, and evaluated a SAW filter using in-house equipment. Although the in-house fabrication method was not suitable for consistent mass production, the rapid design–production–measurement cycle significantly streamlined the development process, making it easier and more cost-effective to create new, effective filters.

Next, we shifted to a higher level in the digital domain, focusing on how packets can avoid collisions among multiple end devices. In this chapter, we specifically concentrated on LoRa, a wireless technology for IoT that shows significant market potential due to its excellent physical properties for resisting environmental noise. However, its public protocol does not support mesh networking and lacks sophisticated MAC methods for collision management. Therefore, we reviewed MAC methods from other wireless technologies, including ALOHA, Slotted ALOHA, and CSMA/CA. Different MAC methods were empirically tested using fabricated end-device units rather than relying solely on computer simulations, and the Packet Delivery Ratio (PDR) was measured to assess the performance of each MAC approach.

Finally, leveraging our understanding of filters and MAC protocols, we conducted a long-term, large-scale deployment test within a commercial building, consisting of 205 end devices and a single gateway distributed across 23 continuous floors. This extensive test demonstrated that the combination of appropriately designed filters and

MAC schemes can deliver a stable IoT network in real-world applications, specifically for centralized water-leakage detection, rather than remaining merely a theoretical discussion within an academic framework.

Throughout the entire study period, I acquired numerous practical skills. For instance, I learned about IC fabrication processes and RF measurement techniques while studying SAW filters, as well as PCB design and fabrication and embedded system programming while developing MAC schemes for LoRa end devices. Additionally, I gained experience in software programming and system integration, and I had the opportunity to collaborate with property engineers during the deployment tests. These valuable experiences equipped me not only with academic knowledge, but also with the ability to translate research outcomes into practical solutions that can make a meaningful impact in society

# 6. RECOMMENDATION

Considering the findings presented in this thesis, several key recommendations can be made to further advance the field of IoT network stability. These suggestions aim to address the identified limitations and guide future research and practical implementation.

In the second section of this thesis, we focused on improving IoT network stability at the hardware component level. Our investigation centered on a SAW filter that effectively eliminates unwanted ambient noise outside the data channel's frequency band. A major contribution of this section is the complete design flow—simulation, fabrication, and measurement—of the SAW filter using only in-house equipment. The entire process was carried out on campus by research students, which minimized time, cost, and manpower, thereby lowering the barrier for iterative SAW filter development.

However, there remains substantial room for further exploration. While a rapid in-house design phase is beneficial, once a promising design is obtained, it should be transferred to the semiconductor industry to finalize the integrated circuit implementation. After demonstrating a functional design with essential features on campus, industry experts should address remaining practical issues, such as optimizing the layout for cost-effective wafer utilization and maximum yield, adjusting the structure to ease fabrication, developing bonding strategies to connect the wafer to the package without degrading RF performance, and selecting packaging solutions compatible with existing PCB designs. Although these industrial steps may not directly advance academic research, they are crucial for ensuring that the designed SAW filters are compatible with highly modularized commercial electronic systems.

Furthermore, the demonstrated in-house fabrication capability is not limited to SAW filters. It can be extended to other domains such as micro-mechanics,

mechatronics, micro-fluidics, and sensor design. These research areas span multiple disciplines, including electronics, biology, and chemistry, and thus encourage cross-departmental collaboration within PolyU. Such interdisciplinary research has strong potential to generate innovative solutions and breakthroughs that have not yet been realized.

In the third section of this research, we focused on enhancing IoT network stability at the software control level. We designed and evaluated a MAC protocol for collision avoidance in LoRa, a promising platform for LPWAN-based IoT applications. The original LoRa MAC relies on a relatively simple ALOHA scheme, which was adequate when devices transmitted short packets infrequently and were well separated in time, making collisions less critical. However, as the number of devices grows beyond one hundred, the limitations of this MAC become evident, with collisions significantly degrading performance. In addition, the lack of an enhanced MAC prevents the original LoRa MAC from supporting mesh networking, leaving collisions among network extenders unresolved. To address these issues, we developed a CSMA/CA-based MAC method adapted from other wireless communication standards, implemented the required hardware, wrote the firmware to realize the CSMA/CA logic, and empirically evaluated its performance.

We identify two major directions to extend this work. First, despite the primitive nature of the current LoRaWAN MAC, our developed MAC scheme could be integrated into the LoRaWAN specifications. These specifications not only define the MAC behavior, particularly collision-avoidance mechanisms, but also standardize packet formats, device type definitions, encryption methods, and network-joining procedures. Integrating our approach into such a framework would support interoperability among LoRaWAN-certified gateways and devices, allowing devices from different vendors to join and switch between networks seamlessly.

Second, our proposed CSMA/CA method depends on assigning unique identifiers to devices within the same coverage area. Our results show that collisions can be effectively avoided if these identifiers are assigned carefully and without repetition, analogous to solving a Sudoku puzzle. However, in the current implementation, the assignments are hardcoded in the firmware, and no dynamic number-assignment mechanism is provided. In real deployments, it is difficult to predict which devices will ultimately fall within each other's RF coverage, and environmental conditions may change over time. Even if the initial configuration is manually optimized, it may become invalid later. Therefore, a mechanism that periodically and automatically verifies whether the identifier assignments remain valid, and reassigns them when necessary, is essential. Developing such an automated checking and reassignment mechanism is a key step toward real-world applicability.

In the final section of this research, we concentrated on the application layer of stable IoT networks. Although the focus of our work is IoT network stability, stability by itself does not directly benefit society; it is the applications enabled by a stable network that create real impact. To this end, we implemented an IoT network and platform for water-leakage detection at the scale of a commercial building. Our deployment features one of the highest numbers of actual devices reported and achieves a near-best packet delivery ratio, demonstrating both practical scalability and robustness.

Future work can extend this application in several ways. While the current system can detect and report water leakage events, its effectiveness still depends on the responsiveness of property management teams. To improve this, we propose integrating actuators into the system, such as electronically controlled water valves on each floor. For example, when a leak is detected on the 15th floor, the system could automatically

close the corresponding valve and simultaneously notify property management, thereby reducing response time and potential damage.

Additionally, the platform can be expanded to interface with existing Building Management Systems (BMS). This could involve adding more sensors to monitor parameters such as noise levels, ambient temperature, and humidity at multiple locations, as well as pump status, fire-safety device health, and electrical metering. Such enhancements would support a transition from traditional, relatively rigid sensing-control infrastructures to a new generation of smart buildings and smart cities, enabled by flexible, scalable, and stable IoT systems.

# Reference


[1] K. Hashimoto, “Surface Acoustic Wave Devices in Telecommunications” Springer: Berlin/Heidelberg, Germany, 2000, ISBN 978-3-642-08659-5.

[2] R. Aigner, “SAW and BAW technologies for RF filter applications: A review of the relative strengths and weaknesses.” In Proceedings of the 2008 IEEE Ultrasonics Symposium, Beijing, China, 2–5 November 2008, pp. 582–589

[3] D. Morgan, Surface Acoustic Wave Filters with Applications to Electronic Communications and Signal Processing, Elsevier, UK (2007).

[4] Y. Kobayashi, T. Tsuchiya, M. Okazaki, Y. Asao, K. Hashimoto, and S. Shikata, “High-frequency surface acoustic wave resonator with ScAlN/hetero-epitaxial diamond,” *Diamond and related materials*, vol. 111, 2021, doi: 10.1016/j.diamond.2020.108190.

[5] Z. Tang, W. Wu, J. Gao, and P. Yang, “Feasibility Study on Wireless Passive SAW Sensor in IoT Enabled Water Distribution System,” in *2017 IEEE International Conference on Internet of Things (iThings) and IEEE Green Computing and Communications (GreenCom) and IEEE Cyber, Physical and Social Computing (CPSCom) and IEEE Smart Data (SmartData)*, 2017, vol. 2018, pp. 830–834, doi: 10.1109/iThings-GreenCom-CPSCom-SmartData.2017.127.

[6] Lv, D. W., Li, X. J., Yang, L. X., Liu, D. J., Xiong, K., Liang, X. B., . . . Zhang, B. (2015). Research on digital substation IOT based on SAW sensing technology. *Applied Mechanics and Materials, 738-739,* 125-128. doi:http://dx.doi.org.ezproxy.lb.polyu.edu.hk/10.4028/www.scientific.net/AMM.738-739.125

[7] K. Hashimoto, G. Endoh and M. Yamaguchi, “Coupling-of-modes modelling for fast and precise simulation of leaky surface acoustic wave devices”. In Proceedings of the 1995 IEEE Ultrasonics Symposium, An International Symposium, Seattle, WA, USA, 7–10 November 1995; Volume 1, pp. 251–256.

[8] J.H. Kuypers and A.P. Pisano “Green’s function analysis of Lamb wave resonators.” In Proceedings of the 2008 IEEE Ultrasonics Symposium, Beijing, China, 2–5 November 2008; pp. 1548–1551

[9] T. Wang, R. Green, R. Guldiken, J. Wang, S. Mohapatra, and S.S. Mohapatra, “Finite Element Analysis for Surface Acoustic Wave Device Characteristic Properties and Sensitivity,” Sensors (Basel, Switzerland), vol. 19, no. 8, p. 1749, 2019, doi: 10.3390/s19081749.

[10] H. Nakahata *et al.*, “Diamond-based surface acoustic wave devices,” *Semiconductor science and technology*, vol. 18, no. 3, pp. S96–S104, 2003

[11] Campbell, C.; Burgess, J.C. Surface AcousticWave Devices and Their Signal Processing Applications. J. Acoust. Soc. Am. 1991, 89, 1479–1480.

[12] J. C. A. Ondo, E. J. J. Blampain, G. N. Mbourou, S. M. Murtry, S. Hage-Ali, and O. Elmazria, "FEM modeling of the temperature influence on the performance of saw sensors operating at gigahertz frequency range and at high temperature up to 500°c," *Sensors (Basel, Switzerland)*, vol. 20, no. 15, pp. 1–14, 2020, doi: 10.3390/s20154166.

[13] M. Z. Aslam, V. Jeoti, S. Karuppanan, A. F. Malik, and A. Iqbal, "FEM analysis of sezawa mode SAW sensor for VOC based on CMOS compatible AlN/SiO2/Si multilayer structure," *Sensors (Basel, Switzerland)*, vol. 18, no. 6, p. 1687, 2018, doi: 10.3390/s18061687.

[14] Y.-G. Zhao, M. Liu, D.-M. Li, J.-J. Li, and J.-B. Niu, "FEM modeling of SAW organic vapor sensors," *Sensors and actuators. A. Physical.*, vol. 154, no. 1, pp. 30–34, 2009, doi: 10.1016/j.sna.2009.07.014.

[15] X. Li, J. Bao, L. Qiu, N. Matsuoka, T. Omori, and K.-Y. Hashimoto, "3D FEM simulation of SAW resonators using hierarchical cascading technique and general purpose graphic processing unit," *Japanese Journal of Applied Physics*, vol. 58, no. SG, p. SGGC05, 2019, doi: 10.7567/1347-4065/ab0ffb.

[16] S. Chen, H. Xu, D. Liu, B. Hu, and H. Wang, "A vision of IoT: Applications, challenges, and opportunities with China perspective," *IEEE Internet Things J.*, vol. 1, no. 4, pp. 349-359, Aug. 2014, doi: 10.1109/JIOT.2014.2337336.

[17] A. Ikpehai *et al.*, "Low-power wide area network technologies for Internet-of-Things: A comparative review," *IEEE Internet Things J.*, vol. 6, no. 2, pp. 2225-2240, Apr. 2019, doi: 10.1109/JIOT.2018.2883728.

[18] S. Al-Sarawi, M. Anbar, K. Alieyan and M. Alzubaidi, "Internet of Things (IoT) communication protocols: review," in *Proc. 8th Int. Conf. Inf. Technol. (ICIT)*, Amman, Jordan, 2017., doi: 10.1109/ICITECH.2017.8079928.

[19] G. A. Akpakwu, B. J. Silva, G. P. Hancke and A. M. Abu-Mahfouz, "A survey on 5G networks for the Internet of Things: Communication technologies and Challenges," *IEEE Access*, vol. 6, pp. 3619-3647, 2018. doi: 10.1109/ACCESS.2017.2779844.

[20] J. Chen, K. Hu, Q. Wang, Y. Sun, Z. Shi and S. He, "Narrowband Internet of Things: Implementations and applications," *IEEE Internet Things J.*, vol. 4, no. 6, pp. 2309-2314, Dec. 2017, doi: 10.1109/JIOT.2017.2764475.

[21] J. de Carvalho Silva, J. J. P. C. Rodrigues, A. M. Alberti, P. Solic, and A. L. L. Aquino, "LoRaWAN—A low power WAN protocol for Internet of Things: A review and opportunities," in *Proc. IEEE Int. Multidiscipl. Conf. Comput. Energy Sci. (SpliTech)*, Jul. 2017, pp. 1-6.

[22] L. K. Baghel, S. Gautam, V. K. Malav, and S. Kumar, “TEMPSENSE: LoRa enabled integrated sensing and localization solution for water quality monitoring,” *IEEE Trans. Instrum. and Meas.*, vol. 71, pp. 1-11, 2022, Art no. 3000311, doi: 10.1109/TIM.2022.3175059.

[23] C. Ebi, F. Schaltegger, A. Rüst, and F. Blumensaat, “Synchronous LoRa mesh network to monitor processes in underground infrastructure,” *IEEE Access*, vol. 7, pp. 57663-57677, 2019, doi: 10.1109/ACCESS.2019.2913985.

[24] H. Lee and K. Ke, “Monitoring of large-area IoT sensors using a LoRa wireless mesh network system: Design and evaluation,” *IEEE Trans. Instrum. and Meas.*, vol. 67, no. 9, pp. 2177-2187, Sept. 2018, doi: 10.1109/TIM.2018.2814082.

[25] N. Dey, A. S. Ashour, F. Shi, S. J. Fong and R. S. Sherratt, "Developing residential wireless sensor networks for ECG healthcare monitoring," *IEEE Trans. Consum. Electron.*, vol. 63, no. 4, pp. 442-449, Nov. 2017, doi: 10.1109/TCE.2017.015063.

[26] P. Chanak and I. Banerjee, "Congestion free routing mechanism for IoT-enabled wireless sensor networks for smart healthcare applications," *IEEE Trans. Consum. Electron.*, vol. 66, no. 3, pp. 223-232, Aug. 2020, doi: 10.1109/TCE.2020.2987433.

[27] P. P. Ray, N. Thapa and D. Dash, "Implementation and performance analysis of interoperable and heterogeneous IoT-edge gateway for pervasive wellness Care," in *IEEE Trans. Consum. Electron.*, vol. 65, no. 4, pp. 464-473, Nov. 2019, doi: 10.1109/TCE.2019.2939494.

[28] W. -J. Chang, L. -B. Chen, I. -C. Lin and Y. -K. Ou, "iBuffet: An AIoT-based intelligent calorie management system for eating buffet meals with calorie intake control," *IEEE Trans. Consum. Electron.*, vol. 67, no. 4, pp. 226-234, Nov. 2021, doi: 10.1109/TCE.2021.3131687.

[29] S. C. Sethuraman, P. Kompally, S. P. Mohanty and U. Choppali, "MyWear: A novel smart garment for automatic continuous vital monitoring," *IEEE Trans. Consum. Electron.*, vol. 67, no. 3, pp. 214-222, Aug. 2021, doi: 10.1109/TCE.2021.3085888.

[30] M. Centenaro, L. Vangelista, A. Zanella and M. Zorzi, “Long-Range communications in unlicensed bands: The rising stars in the IoT and smart city scenarios,” *IEEE Wireless Commun.*, vol. 23, no. 5, pp. 60-67, October 2016, doi: 10.1109/MWC.2016.7721743.

[31] P. Ferrari, E.o Sisinni, P. Bellagente, D. F. Carvalho, A. Depari, A. Flammini, M. Pasetti, S. Rinaldi, and I. Silva, “On the use of LoRaWAN and cloud platforms for diversification of mobility-as-a-service infrastructure in smart city scenarios,”

*IEEE Trans. Instrum. and Meas.*, vol. 71, pp. 1-9, 2022, Art no. 5501109, doi: 10.1109/TIM.2022.3144736.

[32] S. Ali, T. Glass, B. Parr, J. Potgieter, and F. Alam, "Low cost sensor with IoT LoRaWAN connectivity and machine learning-based calibration for air pollution monitoring," *IEEE Trans. Instrum. and Meas.*, vol. 70, pp. 1-11, 2021, Art no. 5500511, doi: 10.1109/TIM.2020.3034109.

[33] L. G. Manzano, H. Boukabache, S. Danzeca, N. Heracleous, F. Murtas, D. Perrin, V. Pirc, A. R. Alfaro, A. Zimmaro, and M. Silari, "An IoT LoRaWAN network for environmental radiation monitoring," *IEEE Trans. Instrum. and Meas.*, vol. 70, pp. 1-12, 2021, Art no. 6008512, doi: 10.1109/TIM.2021.3089776.

[34] "*LoRaWAN 1.1 Specification*", LoRa Alliance, Fremont, CA, USA, Oct. 2017.

[35] G. Zhu, C.-H. Liao, T. Sakdejayont, I.-W. Lai, Y. Narusue and H. Morikawa, "Improving the capacity of a mesh LoRa network by spreading-factor-based network clustering," *IEEE Access*, vol. 7, pp. 21584-21596, 2019, doi: 10.1109/ACCESS.2019.2898239.

[36] K. C. V. G. Macaraeg, C. A. G. Hilario and C. D. C. Ambatali, "LoRa-based mesh network for off-grid emergency communications," in *Proc. IEEE GHTC*, Seattle, WA, USA, 2020, pp. 1-4, doi: 10.1109/GHTC46280.2020.9342944.

[37] V. D. Pham, T. D. Dinh and R. Kirichek, "Method for organizing mesh topology based on LoRa technology," in *Proc. Int. Congr. Mod. Telecommun. Control Syst. Workshops (ICUMT)*, Moscow, Russia, Nov. 2018, pp. 1-6, doi: 10.1109/ICUMT.2018.8631270.

[38] M. N. Ochoa, A. Guizar, M. Maman and A. Duda, "Evaluating LoRa energy efficiency for adaptive betworks: From star to mesh topologies," In *Proc. IEEE 13th Int. Conf. Wireless Mobile Comput., Netw. Commun.*, Rome, Italy, 2017, pp. 1-8, doi: 10.1109/WiMOB.2017.8115793.

[39] "*LoRaWAN 1.0.3 Regional Parameters*," LoRa Alliance, Fremont, CA, USA, Jul. 2018.

[40] F. Van den Abeele, J. Haxhibeqiri, I. Moerman and J. Hoebeke, "Scalability analysis of large-scale LoRaWAN networks in ns-3," *IEEE Internet Things J.*, vol. 4, no. 6, pp. 2186-2198, Dec. 2017, doi: 10.1109/JIOT.2017.2768498.

[41] O. Georgiou and U. Raza, "Low power wide area network analysis: Can LoRa scale?," *IEEE Wireless Commun. Lett.*, vol. 6, no. 2, pp. 162-165, Apr. 2017, doi: 10.1109/LWC.2016.2647247.

[42] K. Mikhaylov, Juha Petaejaejaervi and T. Haenninen, "Analysis of capacity and scalability of the LoRa low power wide area network technology," in *Proc. Euro. Wireless Conf.*, Oulu, Finland, 2016, pp. 1-6.

[43] T. Polonelli, D. Brunelli, A. Marzocchi, and L. Benini, “Slotted ALOHA on LoRaWAN-design, analysis, and deployment,” *Sensors*, vol. 19, no. 4, p. 838, 2019, doi: 10.3390/s19040838.

[44] D. Zorbas and B. O'Flynn, “Autonomous collision-free scheduling for LoRa-based industrial Internet of Things,” *in Proc. 20th Int. Symp. World Wireless Mobile Multimedia Netw. (WoWMoM)*, Washington, DC, USA, 2019, pp. 1-5, doi: 10.1109/WoWMoM.2019.8792975.

[45] A. Baiocchi and F. Ricciato, “Analysis of pure and slotted ALOHA with multi-packet reception and variable packet size,” *IEEE Commun. Lett.*, vol. 22, no. 7, pp. 1482-1485, Jul. 2018, doi: 10.1109/LCOMM.2018.2834360.

[46] C. Pham, “Investigating and experimenting CSMA channel access mechanisms for LoRa IoT networks,” in *Proc. IEEE Wireless Commun. and Netw. Conf. (WCNC)*, Barcelona, Spain, Apr. 2018, pp. 1-6, doi: 10.1109/WCNC.2018.8376997.

[47] C. Pham, “Robust CSMA for long-range LoRa transmissions with image sensing devices,” in *Proc. Wireless Days (WD)*, 2018, pp. 116-122, doi: 10.1109/WD.2018.8361706.

[48] T. To and A. Duda, “Simulation of LoRa in NS-3: Improving LoRa performance with CSMA,” in *Proc. IEEE Int. Conf. Commun. (ICC)*, Kansas City, MO, USA, May 2018, pp. 1-7, doi: 10.1109/ICC.2018.8422800.

[49] L. Beltramelli, A. Mahmood, P. Österberg and M. Gidlund, “LoRa beyond ALOHA: An investigation of alternative random access protocols,” *IEEE Trans. Ind. Infomat.*, vol. 17, no. 5, pp. 3544-3554, May 2021, doi: 10.1109/TII.2020.2977046.

[50] H. Huh and J. Y. Kim, “LoRa-based mesh network for IoT applications,” in *Proc. IEEE 5th World Forum Internet Things (WF-IoT)*, Limerick, Ireland, Apr. 2019, pp. 524-527, doi: 10.1109/WF-IoT.2019.8767242.

[51] V. D. Pham, V. Kisel, R. Kirichek, A. Koucheryavy and A. Shestakov, “Evaluation of A mesh network based on loRa technology,” in *Proc. 23rd Int. Conf. Adv. Commun. Tech. (ICACT)*, PyeongChang, Korea (South), 2021, pp. 1-6, doi: 10.23919/ICACT51234.2021.9370792.